NASA CONTRACTOR REPORT

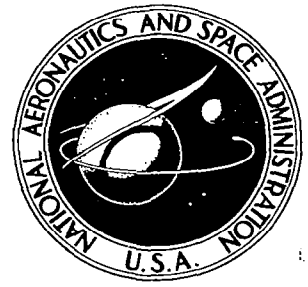

EXPERIMENTAL STUDY OF SUPERLAMINAR FLOW BETWEEN NONCONCENTRIC ROTATING CYLINDERS

by John Vohr

Prepared by
MECHANICAL TECHNOLOGY INCORPORATED
Latham, N. Y.
for Lewis Research Center

NATIONAL AERONAUTICS AND SPACE ADMINISTRATION • WASHINGTON, D. C. • JUNE 1967

NASA CR-749

EXPERIMENTAL STUDY OF SUPERLAMINAR FLOW BETWEEN NONCONCENTRIC ROTATING CYLINDERS

By John Vohr

Prepared under Contract No. NASw-1021 by
MECHANICAL TECHNOLOGY INCORPORATED
Latham, N.Y.

for Lewis Research Center

NATIONAL AERONAUTICS AND SPACE ADMINISTRATION

For sale by the Clearinghouse for Federal Scientific and Technical Information
Springfield, Virginia 22151 – CFSTI price $3.00

FOREWORD

The work described in this report was performed by Mechanical Technology Incorporated under NASA contract NASw-1021. The objective was to investigate the steady-state and dynamic characteristics of two journal bearings, namely the tilting-pad and full floating ring bearings, operating with the lubricant film in the turbulent regime. Also fundamentals of Taylor vortex flow and turbulence in concentric and eccentric annuli were investigated. In previous work, done under NASA contract NASw-771, the steady-state and dynamic properties of basic bearing elements, the partial arc and the full cylindrical bearing, were calculated and compared with experimental measurements in laminar and turbulent flow regimes. Also, investigation of the fundamentals of vortex and turbulence in concentric annuli was begun. This work provided the foundation for the work now being reported on Contract NASw-1021.

The work reported herein was done under the technical management of Joseph P. Joyce, Space Power Systems Division, NASA-Lewis Research Center, with William J. Anderson, Fluid System Components Division, NASA-Lewis Research Center, as research consultant. The report was originally issued as MTI Report 65TR43.

ABSTRACT

An experimental study was made of superlaminar flow in the annular space between a rotating inner cylinder and a close clearance stationary outer cylinder.

The study included: (1) measurements of transition speed for onset of vortices at eccentricity ratios of 0.08, 0.2, 0.35, 0.51, 0.68 and 0.83, (2) measurements of rotational torque in the vortex and turbulent flow regimes over the range of Reynolds numbers from 200 to 4300, and (3) measurements of pressure profiles in the vortex and turbulent flow regimes over the range of Reynolds numbers from 400 to 3200. Critical speed for onset of Taylor vortices was found to increase with eccentricity, this increase being greater at higher clearance ratios than at lower ones. At C/R = 0.099, the critcial speed for onset of vortices at an eccentricity ratio of 0.7 was found to be 2.2 times greater than the critical speed for the case of concentric cylinders. At C/R = 0.0104, the critical speed at $\varepsilon = 0.7$ was 1.5 times greater than that for concentric cylinders.

The measurements made of torque and pressure profiles in the Taylor vortex flow regime were compared with theoretical calculations based on an analysis by DiPrima (Ref. 1). When diPrima's analysis was modified to correct for the discrepancy between theoretical and measured Taylor critical speeds, the theoretical calculations of torque and pressure profiles agreed with measured values to within 10% for speeds up to 1.5 times the critical speed.

Visual studies were made of vortex flow and turbulence in the flow between a rotating inner cylinder and an 80° partial arc outer cylinder. The critical speed for onset of Taylor vortices in the flow were found to agree with theoretical prediction by DiPrima (Ref. 4) to within 25%.

C O N T E N T S

EXPERIMENTAL STUDY OF SUPERLAMINAR FLOW BETWEEN NONCONCENTRIC ROTATING CYLINDERS

by John Vohr

Mechanical Technology Incorporated

SUMMARY

This report describes a fundamental investigation of the nature of Taylor vortex flow and turbulence in concentric and eccentric annuli. The study was intended to complement more direct experimental studies of bearings operating in the superlaminar flow regime. The object of the present work was to gain basic understanding of the nature of superlaminar flow in bearing configurations to help guide efforts to develop a more comprehensive superlaminar flow lubrication theory which would include vortex flow as well as true turbulence.

The test apparatus used in the present study consisted basically of an aluminum rotating inner cylinder, 22 1/4 inches in length, with a diameter of 3.6415 $\pm$ 0.0014 inches. Around this inner cylinder was placed either a close clearance aluminum outer cylinder ($C/R_1 = 0.0104$) or a Plexiglas and aluminum outer cylinder, the latter being used for partial arc studies. Both outer cylinders could be positioned at varying eccentricities about the inner cylinder ranging from the concentric position (eccentricity ratio = 0) to a fully eccentric position (eccentricity ratio = 1.0).

The test fluids used were silicone fluids of different viscosities which permitted operation to Reynolds numbers of 4200 in the close clearance experiments and 32,500 in the case of the partial arc experiments.

With the close clearance cylinders, measurements were made of the critical rotational speeds for onset of vortices in the flow between the cylinders as a function of eccentricity of the cylinders.

Torque measurements were made at different eccentricity ratios in both the vortex flow and turbulent flow regimes and compared with theoretical prediction based on the work of DiPrima (Ref. 1). Measurements were also made of the pressure profiles around the cylinders in vortex and turbulent flow and compared with theoretical prediction.

Visual studies were made with the partial arc rig to determine the nature of vortex and turbulent flow in configurations involving both diverging and converging flow passages.

Among the results obtained in the study was the determination of a curve of critical speed for onset of Taylor vortices applicable to full circular journal bearings. Also, theoretical prediction of torque and pressure profiles in the vortex regime was found to agree quite well with experimental measurements if measured values for critical Taylor numbers were used in the theoretical analysis. Thus, out of the study has come a better understanding of hydrodynamic lubrication applicable to bearings operating at speeds just above the speed at which Taylor vortices form.

INTRODUCTION

G.I. Taylor, in his classical investigation of vortex instability (Ref. 2), showed both theoretically and experimentally that regularly spaced toroidal vortices will develop in the flow between a stationary outer cylinder and a concentric rotating inner cylinder when the parameter $\frac{V_1 C}{\nu}\sqrt{\frac{C}{R_1}}$ attains a value of 41.2. Where

V_1 = surface speed of inner cylinder

R_1 = radius of inner cylinder

C = radial clearance between inner and outer cylinder

ν = fluid kinematic viscosity

In a full journal bearing, which is basically a cylinder rotating within another, a typical value for C/R_1 is 10^{-3}. Substitution of this value into the equation

$$\frac{V_1 C}{\nu}\sqrt{\frac{C}{R_1}} = 41.2 \qquad (1)$$

yields

$$\frac{V_1 C}{\nu} = 1300 \qquad (2)$$

The generally accepted value of Reynolds number for transition to turbulence is in the range from 1500 to 2000. Therefore, in a typical bearing, one could expect vortex flow to occur prior to turbulence.

At the present time, a theoretical method for prediction of bearing performance in the fully turbulent flow regime has been published by Ng and Pan (Ref. 3). Prior to the present investigation, however, there had been no theoretical analyses of bearing performance in the region of vortex flow. Ability to predict bearing performance in vortex flow is of considerable practical importance since this region "bridges the gap" between laminar flow and fully developed turbulence. Consequently, when MTI began to conduct studies of superlaminar flow in bearings, part of the effort was directed toward achieving a thorough basic understanding of vortex flow between concentric and non-concentric cylinders.

The first work done at MTI in the study of vortex flow between non-concentric cylinders was theoretical and concerned the prediction of transition speed for onset of vortices. In the case of non-concentric cylinders, e.g., loaded journal bearings, the analysis of the stability of the flow is complicated by the fact that the radial clearance varies circumferentially and there is a varying circumferential pressure gradient around the cylinders. An analysis of the stability of flow between rotating cylinders with a circumferential pressure gradient had been accomplished by R.C. DiPrima (Ref. 4) and also by others (Refs. 5, 6, and 7). By applying his analysis locally to the flow within a journal bearing, DiPrima (Ref. 8) developed an approximate criterion for the stability of flow in such a bearing. The results of DiPrima's work are presented in Fig. 1. In this figure the critical values of the parameter

$\frac{V_1 C}{\nu}\sqrt{\frac{C}{R_1}}$ for development of vortices at different circumferential positions are plotted vs. eccentricity ratio ε. One can note that the position of least stability is at $\theta = 0$ (point of maximum clearance). When operating with values of eccentricity ratio greater than $\varepsilon = 0.67$, the stability of flow everywhere within a journal bearing should be greater than it was when the journal was concentric.

To obtain experimental verification of DiPrima's analysis, and to obtain a fundamental understanding of the nature of vortex flow between non-concentric cylinders, an experimental study under NASA Contract NASW-771 was made of the flow between a rotating inner cylinder and a stationary glass outer cylinder which could be positioned at different eccentricities. The results of these studies are reported in Reference 9. The studies included determination of transition speeds by means of torque measurements, measurement of friction factors in vortex and turbulent flow regimes, and visual studies of flow in vortex and turbulent flow regimes.

It was found that the transition speeds for onset of vortices, as determined from torque measurements, increased steadily with eccentricity ratio. At an eccentricity ratio of 0.707, the measured Taylor transition speed was 2.2 times that measured for the case of concentric cylinders. These results were not in agreement with DiPrima's minimum stability curve (Fig. 1) which predicted that flow at the point $\theta = 0$ would first become less stable to disturbances of the Taylor type as eccentricity ratio increased from zero, and then would become slightly more stable at eccentricity ratios above 0.67. One possible reason for this lack of agreement between theory and experiment was the relatively large radial clearance between the test cylinders ($C/R_1 = 0.099$). With this clearance, fluid inertia effects could have had a significant effect on the development of vortices in the flow. In view of this possibility, the results of the transition speed tests with the first test cylinders could not be confidently applied directly to journal bearings. Work began under Contract NASW-771 was extended under Contract NASW-1021 to investigate Taylor transition speeds using cylinders of reduced clearance. In addition to determination of transition speed, measurements were also made of pressure profiles and friction factors between close clearance cylinders in the vortex and turbulent flow regime. These measurements were compared with recent theoretical work by DiPrima on vortex flow (Ref. 1) and also with the theory of Ng and Pan (Ref. 3) for turbulent flow. The results of this comparison indicate that DiPrima's analyses provide a good basis for a theory of lubrication in the vortex regime.

In the course of the present studies of superlaminar flow between rotating cylinders, some time was spent exploring the feasibility of using a novel flow visualization technique known as electrochemiluminscence for the study of bearing flow. This technique, which was first investigated in detail by Howland et. al. (Ref. 10), relies on an electrochemical reaction at the surface of a body immersed in flowing solution to display

the boundary layer flow pattern over the body. In the present studies it was demonstrated that Taylor vortices could be displayed by this technique. However, some difficulties were encountered with the technique and further investigation of it was stopped in favor of completing the other types of studies using more conventional methods.

In addition to the studies of flow between close clearance cylinders, visual studies were also made of vortex flow and turbulence in a partial arc configuration. It had previously been assumed that Taylor vortices would develop in a partial arc when sufficiently high speeds were obtained, however, this had never been directly demonstrated. Since many bearings are of a partial-arc configuration (including tilting pad bearings) it was considered of importance to gain a qualitative understanding of the nature of superlaminar flow in such geometries. The present visual studies revealed that clearly defined vortices do develop in the partial-arc configuration at transition speeds which are in fair agreement with theory.

STUDIES OF FLOW BETWEEN CLOSE-CLEARANCE, NON-CONCENTRIC, ROTATING CYLINDERS

Close Clearance-Test Apparatus

The test rig used for the close-clearance, eccentric-cylinder measurements is essentially the same apparatus that was used in the previous work (Ref. 9), but with the original glass outer cylinder replaced by an aluminum cylinder of smaller I.D. A complete description of the apparatus with glass outer cylinder is provided in Ref. 9. The close clearance aluminum outer cylinder used in the present experiments had an I.D. of 3.681 ± 0.0012 inches which, combined with the inner cylinder of 3.6415 ± 0.0014 inches yields a radial clearance of 0.01975 ± 0.026 inch or a C/R_1 ratio of 0.0111. One can note that although the diametrical tolerances on both inner and outer cylinders were reasonably good, the measured value of radial clearance still contains a sizable percentage uncertainty (approximately $\pm$ 13%). To determine C more accurately, the following procedure was used. The test rig was first filled with test fluid so that only the bottom two or three inches on the inner cylinder were immersed. Then the cylinder was rotated at angular speed Ω and the resulting torque, G_o, was measured. Next an accurately measured volume υ of test fluid was added to that already present in the rig bringing the liquid level up to two or three inches below the top of the inner cylinder. Then the inner cylinder was rotated again at speed Ω and the new torque G was measured. The difference in torque $G - G_o$ can be shown to be

$$G - G_o = \frac{4\mu R_1^2 R_2^2 \Omega \upsilon}{(R_1 + R_2)^2 C^2}^{1/2} \tag{3}$$

Solving (3) for C we get:

$$C = \left[\frac{4\mu R_1^2 R_2^2 \Omega \upsilon}{(G-G_o)(R_1+R_2)^2}\right]^{1/2} \tag{4}$$

All the quantities within the parentheses on the right hand side of Eq. (4) could be determined with excellent accuracy, the least certain quantities being the torque difference $G - G_o$ and the fluid viscosity μ, each of which were known to within $\pm$ 2%. Thus, C could be determined from Eq. (4) to an accuracy of $\pm$ 2%. The value of C determined in this fashion was $C = 0.0190 \pm 0.0004$ inches. The corresponding value for C/R_1 is 0.0104.

The close-clearance aluminum outer cylinder contained 16 circumferential pressure taps with an angular spacing between each tap of 22-1/2°. The taps were arranged in a spiral so that the wake from one tap would not affect the pressure reading at a following tap. The pressure at each tap was measured

by means of a "U" tube manometer bank with water as the indicating fluid. Since the test fluid used for pressure measurements was two centistoke silicone fluid with specific gravity equal to 0.871, and since this test fluid was over the water in the manometer tubes, each inch of manometer reading corresponded to a pressure of 0.129 inches of water.

The torque between the rotating cylinders was measured by the method described in Ref. 9. This method consisted of using weights to exactly counterbalance the torque transmitted to the outer cylinder.

The test fluid used for torque measurements was a silicone fluid of one centistoke viscosity at 77 F. The viscosity of this fluid as well as that of the two centistoke fluid mentioned above was measured carefully with a Cannon - Fenske viscometer at different temperatures. During each test run, the ambient temperature was measured, and since fractional heating in the test rig was negligible at speeds up to the Taylor transition speed, it was assumed that the fluid in the test rig was at ambient temperature. This was verified at the end of each run by drawing the fluid from the test apparatus and measuring its temperature. Viscosity variation with temperature was taken into account in all of the data obtained. It is believed that during each test run, the fluid viscosity was known accurately to within 1%.

Measurement of Transition Speed for Onset of Vortices

In Fig. 2 is shown a typical torque versus speed curve for the case of concentric cylinders. Up to a rotation speed of 2.875 rps, torque is linearly proportional to speed, characteristic of laminar flow. At the transitional speed of 2.875 rps, the torque curve suffers a sharp discontinuity in slope indicative of the onset of vortices. The particular curve shown in Fig. 2 is for the clearance ratio $C/R_1 = 0.0104$, however, the torque curves obtained for concentric cylinders with clearance ratio $C/R_1 = 0.099$ have nearly the same shape as those measured for the smaller clearance.

In the case of eccentric cylinders, the torque versus rotational speed curve has the same basic characteristics as those obtained for concentric cylinders. However, as eccentricity ratio increases, the change in slope of the torque curve at Taylor transition speed becomes less pronounced, indicating a more gradual transition to vortex flow. Also, the transition speed for onset of vortices increases as eccentricity increases. These general features of flow between non-concentric cylinders were all observed in the earlier experiments using cylinders with relatively large clearance ratio ($C/R_1 = 0.099$). In these earlier measurements, the increase in Taylor transition speed due to increase in eccentricity was considerably greater than that predicted by DiPrima's approximate analysis (Ref. 8). It was thought that part of this discrepancy may have been due to inertia effects, which could have been appreciable at the clearance ratio tested. To try to resolve this question, the present experiments were performed using the reduced clearance ratio $C/R_1 = 0.0104$.

Some typical torque versus speed curves for $C/R_1 = 0.0104$ are shown in Figs. 3 through 6. These curves are similar to those obtained previously with $C/R_1 = 0.099$ except for two differences; (1) the increase in transition speed with eccentricity is not as great at the lower clearance ratio as it was at the larger clearance ratio, and (2) the change in slope of the torque versus speed curve at the point of onset of vortices is less pronounced at the lower clearance ratio. This latter feature can be seen by comparing Fig. 4 with Fig. 7, the latter taken from Ref. 9. The former feature can be seen in Fig. 8 where the measured transition speeds for onset of vortices are plotted as a function of eccentricity for the two clearance ratios tested. Shown also is the theoretical curve obtained by DiPrima indicating the speed at which velocity profiles at $\theta = 0^o$ first become unstable to disturbances of the Taylor vortex type. Transition speed is plotted in terms of the dimensionless parameter

$$\frac{V_1 C}{\nu} \sqrt{\frac{2C}{R_1 + R_2}} = \sqrt{1/2\ T}$$

where T is the usual Taylor number for the case of outer cylinder stationary.

One should note that DiPrima's analysis pertains to the case $R_1/R_2 \longrightarrow 1$, which is the reason why the simpler parameter

$$\frac{V_1 C}{\nu}\sqrt{\frac{C}{R_1}}$$

was used in Fig. 1

It can be seen from Fig. 8 that transition speed for onset of vortices between non-concentric cylinders does depend significantly on clearance ratio for values of C/R_1 between 0.0104 and 0.099. As has been noted earlier, the most likely reason for this dependence would seem to be the effect of fluid inertia. If one considers the equations of motion governing the flow around concentric cylinders one can show that the ratio of inertia terms to viscous terms can be expressed by the dimensionless grouping*

$$\frac{V_1 C}{\nu}\sqrt{\frac{C}{R_1}}$$

At the point of onset of vortices, we know that the dimensionless grouping

$$\frac{V_1 C}{\nu}\sqrt{\frac{C}{R_1}}$$

has a value of approximately 41.2. Therefore, at the point of onset of vortices, the ratio of the magnitude of inertia terms to viscous terms would be given by $41.2\sqrt{\frac{C}{R_1}}$. For $C/R_1 = 0.099$ this ratio would be approximately 13, which is certainly not negligible.

Inertia effects could influence the stability of flow between non-concentric cylinders in two different ways. One way is through the effect of inertia on the shape of the flow velocity profiles. The analysis of the stability of velocity profiles in which inertia forces are taken into account is such a difficult problem, however, that it is difficult to estimate whether this effect of inertia would be a destabilizing or stabilizing one.

A second way in which inertia forces could effect the apparent stability of flow between non-concentric cylinders is by retarding the rate of growth of vortices in those regions where flow is unstable. Let us consider a situation in which the flow is unstable over a 30^o arc segment of the circumference. This means that infinitesimal disturbances of the Taylor type in the flow would tend to grow during the period in which they are swept through this arc segment. If, however, inertia forces in the flow were quite strong compared with viscous forces, the growth of the above mentioned disturbances might be significantly

*This is demonstrated in Ref. 11

retarded and the point of measurable instability of the flow could be prolonged until the flow was unstable over a greater fraction of the circumference.

There is some evidence that inertia effects did influence the growth of vortices in the way described above in the large clearance tests. For one thing, in the visual studies of vortex flow performed at $C/R_1 = 0.099$ it was observed that the point where the vortices appeared to be strongest was some 50^o downstream of the point of maximum instability. Also, the fact that for the larger clearance ratio, the change in the slope of the torque versus speed curve at onset of vortices was more abrupt than it was for smaller clearance ratio can be explained in terms of inertia effect. If inertia effects do cause the development of vortices to be delayed until a large fraction of the flow is unstable, then it would seem reasonable to expect that when the vortices do finally develop in the flow, the transition would be an abrupt one.

It might be well to point out at this time that the absence of scatter in the measurements of transition speed at $C/R_1 = 0.099$ was due in part to the fact that the discontinuity in the torque versus speed curves was an abrupt one. On the other hand, at $C/R_1 = 0.0104$, the relative gradualness of the transition to vortex flow make it difficult to determine transition speed precisely, which resulted in the experimental scatter for measurements of transition speed at this clearance ratio.

From an examination of the transition speed data in Fig. 8, one is tempted to conclude that in the limit as C/R_1 goes to zero, transition speeds for onset of vortices would be correctly predicted by DiPrima's theoretical curve. This may not be so, however, since this theoretical curve pertains only to local stability at each circumferential cross section without consideration of the effect that differing upstream or downstream flow conditions may have on flow stability at the point in question. A vortex tube in a viscous fluid cannot end within the body of the fluid but must either close upon itself in a toroidal shape or must end on solid boundaries. Visual observations of vortices in flow between non-concentric cylinders have shown the vortices run continuously around the cylinders. Presumably, then, for a vortex to develop at any circumferential position, the vortex must extend upstream and downstream and its development must depend on the flow conditions it meets in these two directions. It can be argued that in the limit as C/R_1 goes to zero, the effect of upstream and downstream conditions on local stability should become negligible. This, however, has not been rigorously proven and probably will not be until a analysis of the stability problem is performed taking account of the circumferential variation of velocity profile and pressure gradient.

It is still possible to draw some definite conclusions concerning the stability of flow in a journal bearing where clearance ratios are on the order of 10^{-3}. For one thing, it seems safe to conclude that at speeds below DiPrima's theoretical curve, the flow in the bearing will definitely be stable. DiPrima's curve represents, essentially a conservative stability criteria in that it corresponds to the condition that velocity profiles everywhere in the fluid film be locally stable to all disturbances of the Taylor type. On the other hand, the experimental data taken indicates that flow between eccentric cylinders at clearance ratios less than 10^{-2} will

develop vortices at or before the transition speeds given by the curve for $C/R_1 = 0.0104$. Actual onset of vortices in journal bearings will therefore be expected to occur somewhere in the range of speeds between DiPrima's theoretical curve and the experimental curve measured for $C/R_1 = 0.0104$. Evidence provided by measurements of pressure profiles, to be discussed later, indicate that at $C/R_1 = 0.0104$, the development of vortices is no longer significantly affected by fluid inertia. On the basis of the evidence it is believed that the transition speed curve measured at $C/R_1 = 0.0104$ does represent the lower limit of stability for vanishingly small clearance, and hence will apply directly to bearings.

Measurement of Viscous Frictional Drag

Torque measurements were made for flow between rotating cylinders at accentricity ratios of ϵ = 0.08, 0.20, 0.35, 0.51, 0.68 and 0.83 for Reynolds numbers up to 4000. Measurements were made in the laminar flow regime, in the vortex flow regime, and in the turbulent plus vortices regime. In the laminar flow regime, the measured values of torque, G, agreed very well with values predicted by Sommerfeld theory. (Ref. 12). This can be seen in Fig. 9. The Sommerfeld theory is for the case of infinitely long cylinders in that it considers flow in the circumferential direction only. Applied to cylinders of length, L, Sommerfeld theory gives the following expression for torque G_L

$$G_L = \frac{4\pi \mu R_1^2 R_2^2 L}{(R_2-R_1)(R_2+R_1)} \quad \frac{2(1+2\epsilon^2)}{(2+\epsilon^2)(1-\epsilon^2)^{1/2}} \quad \Omega \qquad (5)$$

In the MTI experiments, the length to diameter ratio of the cylinders was 6.12. On the basis of the agreement between measured torque and Sommerfeld theory, it appears that the L/D of 6.12 provides a reasonable approximation to the case of infinitely long cylinders. Only at the highest eccentricity ratio (ϵ = 0.83) do the measured torque values appear to lie slightly below the Sommerfeld curve, indicating some effect of axial flow at the ends of the test cylinders.

In the region of vortex flow, the increase in torque due to development of vortices can be approximately predicted by use of an analysis by DiPrima. (Ref. 1). This analysis enables one to calculate the surface shear stress for flow between rotating concentric cylinders with a constant circumferential pressure gradient at speeds just above Taylor transition speed. In the case of non-concentric cylinders, the circumferential pressure gradient varies from point to point. However, by applying DiPrima's analysis locally at each point and numerically summing the results of each local shear stress calculation, the total torque associated with rotating non-concentric cylinders can be approximately determined. The method of calculation is described in more detail in Appendix A. Typical results of the calculations are shown in Fig. 10. The ordinate in this plot is the dimensionless ratio G/G_L where G_L is the theoretical laminar torque predicted by Sommerfeld theory (Eq.(5)). The abscissa is the transition speed parameter $\frac{V_1}{\nu}\frac{C}{\sqrt{\frac{C}{R_1}}}$. Up to the point of onset of vortices, G/G_L is unity. With onset of vortices, G/G_L abruptly begins to increase above unity. For ϵ = 0, the rate of increase of G/G_L is very sharp. As eccentricity ratio increases, the development of vortices in the flow occurs more gradually which is reflected in a more gradual rate of increase for G/G_L.

In Fig. 11 the theoretical curve for G/G_L is compared with measurements made at $C/R_1 = 0.0104$ and 0.099 for the case of concentric cylinders*. The transition value of Taylor number is slightly different for these two clearance ratios ($T_c = 3390$ for $C/R_1 = 0.0107$ and $T_c = 3630$ for $C/R_1 = 0.099$). Therefore, to make the data coincide, the ratio $(T/T_c)^{\frac{1}{2}}$ was used as the abscissa. As can be seen, agreement between theory and experiment is quite good at speeds just above Taylor transition speed.

Measured values for G/G_L at an eccentricity ratio of $\varepsilon = 0.5$ are compared with the theoretical curve in Fig. 12. Data from four separate runs at $C/R_1 = 0.0104$ are shown. For $C/R_1 = 0.099$, data from only one run are shown. The first thing one can notice in Fig. 12 is the difference between the theoretical and measured speeds for onset of vortices. In order to compare the predicted rate of increase of G/G_L with measured rate, it is necessary to shift the theoretical transition point to coincide with the different measured transition points. This was accomplished by using experimental values of T_c in the calculated curves for G/G_L vs. $(T/T_c)^{\frac{1}{2}}$ rather than theoretical values. This was done both for the case of $C/R_1 = 0.0104$ (dashed curve marked 1) and for the case of $C/R_1 = 0.099$ (dashed curve marked 2). In the former instance, the rate of increase of G/G_L at speeds just above Taylor transition speed is generally in good agreement with the theoretical rate although there is some scatter in the data. At $C/R_1 = 0.099$, however, the measured rate of increase in G/G_L is significantly greater than is predicted. As noted earlier, this more abrupt increase in torque at transition point is in keeping with the theory that inertia effects are responsible for the delay in onset of vortices at large clearance ratios.

In Fig. 13 are plotted measured friction factor data for flow between concentric cylinders. The friction factor λ is defined as

$$\lambda = \frac{G}{\pi L \rho V^2 R_1^2} = \frac{2\tau}{\rho V_1^2} \qquad (6)$$

where τ is the surface shear stress on the inner cylinder. For flow between cylinders with inner cylinder rotating, λ is a function of both Reynolds number and C/R_1. The dependence of λ on these parameters is expressed with good accuracy by the following empirical formulae suggested by Wendt (Ref.13)**.

$$\lambda = 0.46\left[\frac{(R_2-R_1)R_2}{R_1^2}\right]^{\frac{1}{4}} (N_{Re})^{-0.5} \; ; \quad \left(80\,\frac{C}{R_1} < N_{Re} < 10^4\right) \qquad (7)$$

$$\lambda = 0.073\left[\frac{(R_2-R_1)R_2}{R_1^2}\right]^{\frac{1}{4}} (N_{Re})^{-0.3} \; ; \quad \left(10^4 < N_{Re} < 10^5\right) \qquad (8)$$

*Actually, the data for $C/R_1 = 0.0104$ is for $\varepsilon = 0.08$. This may account for the fact that this data is not in quite as good agreement with theory as is the data for $C/R_1 = 0.099$.

**The range of Reynolds numbers over which these formulae are to be used has been modified slightly by the writer.

The formulae are based on measurements made by Wendt at clearance ratios of 0.069, 0.176 and 0.47. Values of λ predicted by these formulae for a clearance ratio of 0.099 are plotted as the solid curve in Fig. 13. This curve is in excellent agreement with values of λ measured at C/R_1 = 0.099 (Ref. 9) and with the current data measured at C/R_1 = 0.0104*. The latter data are corrected for clearance ratio effect by means of Wendt's relation

$$\lambda \propto \left[\frac{(R_2-R_1)R_2}{R_1^2}\right]^{\frac{1}{4}} \tag{9}$$

so that they may be compared with the data taken at C/R_1 = 0.099.

Also shown in Fig. 13 is a dashed curve representing data measured by Smith and Fuller (Ref. 14) for a journal bearing having C/R_1 = .00293. This data is also corrected to a clearance ratio of 0.099 by means of the proportionality relation given above. As can be seen, the corrected Smith and Fuller data lie somewhat above the MTI data and the empirical curve of Wendt. However, in view of the accuracy with which Wendt's formulae correlate both his data and the data at MTI, it is recommended that they be used for all clearances.

In Fig. 14 are plotted values of friction factor for flow between cylinders with C/R_1 = 0.0104 at different eccentricity ratios. In Fig. 15 is presented a similar plot for cylinders with C/R_1 = 0.099. Both plots show generally the same features. In the laminar region, λ is inversely proportional to N_{Re}. At the Taylor transition speed, λ departs from the laminar curve and starts to decrease much less slowly with N_{Re}. An interesting feature in the region just above transition speed is that, at a given speed, torque may be greater for ε = 0 than for values of ε around 0.3 or 0.5. This can be seen from the data points in Fig. 14 in the range $550 < N_{Re} < 1100$.

The fact that torque may actually decrease with eccentricity at speeds above Taylor transition speed was also observed by Smith and Fuller (Ref.14) in their experiments.

At high Reynolds numbers the λ curves at different eccentricities again become roughly parallel. The increase in λ with eccentricity, however, is much less pronounced in turbulent flow than in laminar flow. This is shown in Fig. 16 where the ratio of λ at a given eccentricity to λ at ε = 0 is plotted vs. ε. To calculate the torque for fully turbulent flow between eccentric rotating cylinders having large L/D ratios (L/D > 2) and having complete fluid films, it is recommended that Wendt's empirical formulae be used to calculate λ for concentric cylinders, and that this value of λ be increased by the appropriate factor given by the dashed line in Fig. 16. If the L/D of the cylinders is small (L/D < 2) and/or a complete fluid film does not exist between the cylinders, then the above calculations for λ will be conservatively high.

---

*
The data for C/R_1 = 0.0104 are actually taken at an eccentricity ratio of 0.08 rather than zero. This should not affect the friction factor curve significantly however.

Measurement of Pressure Distribution

The classical Sommerfeld solution (Ref. 12) for the velocity distribution and pressure profile around rotating, non-concentric cylinders is based on the following assumptions:

1. The thickness of the fluid film, y, is very small compared to the radius R and length L of the cylinders.

2. There is no variation of pressure across the film.

3. The flow is laminar.

4. Fluid inertia is small compared with viscous shear.

5. Compared with the velocity gradient, dV/dy, all other velocity gradients are negligible (V is the velocity in the circumferential direction).

The first four of these assumptions are generally very well met if the clearance ratio for the cylinders is of the order of 10^{-3} or smaller. Furthermore, if the cylinders have a length to diameter ratio of six or greater, assumption five will be very well satisfied at the axial midplane of the cylinders.

The Sommerfeld pressure distribution for $\epsilon = 0.68$ is shown in normalized form in Fig. 17a and 17b. A characteristic of this solution is that the pressure distribution is antisymmetrical in θ about the point of minimum clearance between cylinders ($\theta = 180^{o}$) and also about the point of maximum clearance ($\theta = 0^{o}$). The velocity distribution and pressure gradient, on the other hand are symmetrical about $\theta = 180^{o}$ and $\theta = 0^{o}$. If the direction of rotation of the inner cylinder changes sign, then the pressure, pressure gradient, and velocity distribution all change sign.

In the close-clearance test rig used at MTI for pressure distribution measurements, the clearance ratio was approximately 10^{-2} (0.0104 to be exact). At this clearance ratio, and at the Reynolds numbers in the tests, one would expect that assumption 4 above would not be fulfilled, that is, one would expect some influence of inertia effects on the pressure distribution. Experience tells us that this effect will probably be slight, e.g., 10 percent of the effect of viscous terms. Assuming this to be so, then the effect of the inertia terms can be approximately determined in the following way.

In the equation of motion relating pressure gradient $\frac{\partial P}{\partial \theta}$ to inertia terms and viscous terms, the inertia terms are of the form $V \frac{dV}{d\theta}$ where V is the component of velocity in the θ direction. (Same as circumferential direction). If inertia terms are of only secondary influence compared with viscous terms, then one can use the Sommerfeld solution for the velocity distribution V in order to approximately evaluate the term $V \frac{dV}{d\theta}$. The term $V \frac{dV}{d\theta}$, calculated

in this manner, can then be used as a first order correction to the Sommerfeld solution for the pressure gradient. If the effect of inertia terms on the pressure distribution is of the order of 10 percent of the effect of the viscous terms, then the resulting pressure distribution, corrected by this approximate method, should be accurate to the order of one percent.

It is important to note that since the Sommerfeld solution for V is symmetrical about $\theta = 190^{o}$ and the solution for $\frac{\partial V}{\partial \theta}$ is antisymmetrical the inertia term correction to $\frac{\partial P}{\partial \theta}$ will be antisymmetrical about $\theta = 180^{o}$. When the pressure gradient $\frac{dP}{d\theta}$ is integrated to obtain the pressure distribution P, the inertia term correction to P will be symmetrical about $\theta = 180^{o}$ (integrals of antisymmetrical terms are symmetrical and vice versa). This is illustrated schematically in Fig. 17a. The solid line represents the uncorrected Sommerfeld solution for P while the dashed line represents the pressure distribution with the first order correction for inertia effects.

Next, let us consider how a change in the direction of rotation will effect the first order inertia correction to the pressure distribution. As noted above, changing direction of rotation will change the sign of the Sommerfeld pressure distribution P and the sign of the velocity V. However, since the inertia term $V \frac{dV}{d\theta}$ involves the square of the velocity, its sign <u>will not</u> change with a change in direction of rotation. The uncorrected and corrected pressure distributions *for the case of negative rotation are shown as the solid and dashed lines in* Fig. 17b. Note that the sign of the inertia correction is the same as in Fig. 17a.

From an inspection of Figs. 17a and 17b it is easy to see that if one first measured the pressure distribution for positive rotation including inertia effects, then measured the pressure distribution for negative rotation including inertia effects, and then subtracted one of these pressure distributions from the other, the first order inertia terms would be eliminated and one would be left with a pressure distribution which was due only to viscous effects. This would be true, of course, only if the inertia correction to the pressure distribution were small enough to be accurately calculable by the first order approximation method described above. However, by comparing either of the pressure distributions which include inertia effects with the purely viscous pressure distribution, one can check to see if: (a) the inertia terms do contribute only a small correction to the basic viscous pressure distribution and (b) this correction is symmetrical about $\theta = 180^{o}$. If both (a) and (b) are met, then the validity of the first order correction approach is verified.

In the measurements of pressure profiles made at MTI, the pressure distribution attributable to purely viscous effects was determined by the procedure described above. That is, the pressure profile was measured first

with rotation in the positive direction, then with rotation in the negative direction, and then the second profile was subtracted from the first. Our purpose in eliminating inertia effects from the pressure profiles was two-fold. First, by comparing the purely viscous profile with a profile containing inertia effects one could determine exactly the magnitude of the inertia effects. Secondly, at MTI, analyses have been developed for calculating the effect of turbulence and vortex flow on the viscous shear stress in bearing flows. To compare these analyses with experiment, it was necessary to eliminate inertia effects from the measured pressure profiles.

In Fig. 18 is shown a viscous pressure profile measured at an eccentricity ratio of 0.68 and a Reynolds number of 1660. This is well above the transition Reynolds number for onset of Taylor vortices (N_{Re} = 575) so that this curve would correspond to fully-developed vortex flow with, perhaps, some turbulence. Shown also in Fig. 18 is the pressure profile including the effects of inertia. Both profiles are made dimensionless by dividing by the factor $6\mu V_1 R_1/c^2$. Along the horizontal axis in Fig. 18 is plotted the magnitude of the inertia correction. As can be seen, this correction is both relatively small ($\approx$ 20% of the peak pressure) and is also symmetrical about $\theta = 180^o$ as would be predicted by first order approximation. This indicates that the first order approach to eliminating inertia terms from the pressure profiles in these tests is valid for a Reynolds number of 1660. Since the ratio of inertia terms to viscous terms is proportional to Reynolds number, then this first order approach should be valid for all pressure profiles measured at $N_{Re} < 1660$.

Before leaving Fig. 18, it should be pointed out that the fact that the complete pressure profile can be separated into an antisymmetrical viscous profile and a symmetrical inertia correction indicates that the influence of vortices and turbulence on velocity and shear stress in the flow must be symmetrical about $\theta = 180^o$. This symmetry of flow instability would be theoretically expected to prevail if, and only if, the development of vortices and turbulence depended upon local flow conditions and was not significantly influenced by inertia effects. This being apparently the case, then one would expect that the measured speeds for onset of vortices also would not have been influenced by inertia effect. It therefore follows that the transition speed data measured for $C/R_1 = 0.0104$ should be valid for smaller clearance ratios.

In Fig. 19 are shown two dimensionless pressure profiles measured at an eccentricity ratio of 0.51. Inertia effects have been eliminated from each profile by the procedure described above. The lower profile was measured in the laminar flow regime. As can be seen, the measurements are in virtually perfect agreement with Sommerfeld theory. This was typical of all the laminar flow profiles measured at ϵ = 0.20, 0.35, 0.51, 0.68 and 0.83. This attests not only to the accuracy of the pressure measurements but also to the validity of the concept that the inertia terms contribute a symmetrical first order correction to the viscous pressure profile which can be separated out from the viscous contribution.

The upper pressure profile in Fig. 19 was measured for fully-developed vortex flow. The principal effect of the development of vortice is to increase the magnitude of the peak pressure. The presence of vortices also alters the shape of the profile slightly as will be shown later.

The dashed line in Fig. 19 represents the theoretical prediction of the pressure profile in the vortex flow regine at the value of Taylor number for which the vortex flow measurements were made. Calculations of this theoretical profile was based on DiPrima's (Ref. 1) calculations of the effect of vortex motion on the relation between pressure gradient, net mean flow and shear stress for rotating concentric cylinders. DiPrima's analysis has already been mentioned in the section on frictional drag measurement and the application of DiPrima's analysis to non-concentric cylinders is discussed in detail in Appendix A. As can be seen, the theoretically predicted vortex pressure profile is in good agreement with measured values. The theory predicts that the strength of vortex motion between non-concentric cylinders would be symmetrical about the position of minimum clearance ($\theta = 180^{o}$). As pointed out earlier, measured viscous pressure profiles in the vortex regime confirm this.

In Fig. 20 are shown viscous pressure profiles measured in the laminar and vortex regimes at an eccentricity ratio of 0.68. One can again notice the excellent agreement with Sommerfeld theory in the laminar regime. In the vortex regime, the theoretical profile is somewhat above the measured profile at the lower Taylor number and somewhat above it at the higher Taylor number.

The effect of vortex motion and turbulence on the shape of pressure profiles is shown in Figs. 21, 22 and 23. Here the pressure profiles shown in Figs. 21 and 22 have all been normalized to a peak value of 1.0 to compare their shapes with that of the Sommerfeld profile. Theoretically predicted profile shapes for vortex flow are also drawn in for comparison with experiment. In Fig. 23 there is also presented a theoretical profile based on the turbulent lubrication theory of Ng and Pan (Ref. 3).

The effect of vortex motion and of turbulence is to "straighten out" the pressure profiles in the regions where the pressure gradient is positive. The location of the maximum and minimum peaks of the pressure profiles also tend to shift away from the position of minimum clearance. Both of these effects are exhibited by both the experimental measurements and the theoretical curves. In general, there is good agreement between theory and experiment with regard to the shape of the pressure profiles at super-laminar speeds.

The most significant effect of vortex motion and turbulence on pressure is that of increasing the magnitudes of the peak pressures obtained. This effect is illustrated in Fig. 24, where the peak pressure ratio $P_{max}/(P_L)_{max}$ is plotted vs Reynolds number for cylinders at different eccentricity ratios. P_{max} is the measured or theoretical peak pressure for super-laminar flow while $(P_L)_{max}$ is the peak pressure calculated assuming laminar flow to prevail. Experimental data are shown for eccentricity ratios of 0.20, 0.35, 0.51 and 0.68.

For $\varepsilon = 0.20$, 0.35 and 0.51, the peak pressure ratio $P_{max}/(P_L)_{max}$ increases approximately linearly with Reynolds number from the point of onset of vortices. The transition Reynolds numbers for these three eccentricities are reasonably close together and the rate of increase of $P_{max}/(P_L)_{max}$ is about the same, so that the experimental points for these three eccentricities all fall on approximately the same line. It is interesting to note that the turbulent theory devoloped by Ng and Pan (Ref. 3) also predicts that the value of $P_{max}/(P_L)_{max}$ would be the same for both $\varepsilon = 0.20$ and $\varepsilon = 0.35$ over the range of Reynolds numbers shown. As can be seen in Fig. 24, the agreement between this turbulent theory and experiment is good at Reynolds numbers over 2400 where the theory would be expected to apply.

In Fig. 25, values of the ratio $P_{max}/(P_L)_{max}$ for $\varepsilon = 0.51$ and 0.68 are compared with theoretical curves based on the calculations by DiPrima (Ref. 1). As was the case with torque measurements, agreement between vortex flow theory and experiment is not very good if theoretical values for transition Reynolds numbers are used. On the other hand, if the theoretical curves for $P_{max}/(P_L)_{max}$ are shifted to conform with the measured transition Reynolds numbers, then the agreement between predicted rate of increase of $P_{max}/(P_L)_{max}$ and measured rate of increase is quite good at speeds just above Taylor transition speed. The shifting of curves was accomplished by noting that $P_{max}/(P_L)_{max}$ could be expressed as a function of the dimensionless ratio $N_{Re}/(N_{Re})_{critical}$, where $(N_{Re})_{critical}$ is the value of N_{Re} for first onset of vortices in the flow. The calculation of $P_{max}/(P_L)_{max}$ at different Reynolds number was then done by using experimental values of $(N_{Re})_{critical}$ in this dimensionless ratio rather than theoretical values. The curves obtained in this way are shown in Fig. 25 as the dashed curves labeled corrected theory.

VISUAL STUDIES OF SUPERLAMINAR FLOW USING A PARTIAL ARC OUTER CYLINDER

Partial-Arc Apparatus

In addition to the quantitative measurements made of superlaminar flow between rotating, non-concentric cylinders, visual studies were also made of superlaminar flow in the clearance space between a rotating inner cylinder and a transparent, 80 degree, partial-arc "bearing". The test apparatus for these visual studies is shown schematically in Fig. 26 and a photograph of the apparatus is shown in Fig. 27. The rotating inner cylinder was the one used in the close-clearance test rig described earlier. The outer cylinder consisted of a large bore aluminum tube (I.D. = 4.56") inside of which was cemented an 80 degree arc of Plexiglas, .34 inches thick. The inner surface of this Plexiglas "bearing" was machined concentric with the bore of the outer aluminum tube. The end flanges used in the close-clearance test rig were fitted to this partial-arc rig so that the rotating inner cylinder could be positioned at various eccentricities within the outer tube. When in the concentric position, the radial clearance between the inner cylinder and the Plexiglas partial arc was 0.155 $\pm$ .001 inch while the radial clearance between the inner cylinder and the outer tube was 0.460 inches. Clearance ratio, C/R_1, was 0.0635. When the inner cylinder was eccentrically positioned within the outer tube, the Plexiglas arc could be located at various circumferential positions so that the clearance passage between the arc and the inner cylinder could be either fully converging in the direction or rotation or fully diverging or converging - diverging. The location of the leading edge of the Plexiglas arc with respect to the point of maximum clearance between the inner cylinder and outer tube is indicated by the angle β in Fig. 26.

Viewing of the flow in the partial arc segment was made possible by windows cut in the outer aluminum tube as shown in Figs. 26 and 27. Visualization of flow patterns was accomplished by means of fine aluminum particles, of the type used in paint pigment, suspended in the ten centistoke silicone test fluid.

Description of Flow Patterns

In Fig. 28 is shown a typical sequence of developing vortex flow for the case of a converging partial arc. In this particular case, the eccentricity ratio is 0.706*. β, the angular position of the leading edge of the Plexiglas arc, is 100 degrees, i.e., the trailing edge of the arc is located at the point of minimum clearance between inner cylinder and outer tube. In the first picture in Fig. 28, the flow is entirely laminar. The view shown is a closeup of the leading section of the partial arc. Flow is from right to left as one looks at the photo. Between the right-hand side of the arc and the vertical metal tie rod that can be seen in the photo there is about 50 degrees of arc, i.e., a little over half of the bearing.

---

*Eccentricity ratio is defined as e/C where e is the linear eccentricity of the inner cylinder within the outer cylinder and C is the concentric radial clearance between the inner cylinder and the plexiglas arc.

In the second photo of the sequence, the first substantial signs of the development of Taylor vortices can be seen at the beginning of the arc. As will be discussed later, the flow is least stable at this point because clearance is widest there.

In the third photo in the sequence, Taylor vortex flow is now firmly established. The final photo in Fig. 28 shows the Taylor vortices at an even higher speed where they are even more clearly developed.

The flow pattern of the streamlines in fully developed Taylor flow in the partial arc bearing is shown schematically in Fig. 29. The situation depicted is essentially the same as that shown in Fig. 28(d). Between each solid horizontal line is contained a pair of Taylor vortex tubes. Along each dashed horizontal line fluid is pumped out from the surface of the inner rotating cylinder. This fluid returns to the inner cylinder at each dark horizontal line. At the start of the arc, the flow streamlines are curved back as a result of the positive pressure gradient in this region. At the end of the arc, the pressure gradient is negative and the streamlines continue in the direction of rotation.

The pictures of flow shown in Fig. 28 are typical for the case of a converging partial arc ($\beta = 100^{o}$). In the case of converging - diverging arcs ($\beta = 135^{o}$), the appearance of the flow was similar except that the vortices appeared to be of fairly uniform strength over the length of the arc rather than strongest at the start as was the case at $\beta = 100^{o}$. For fully divergent arcs ($\beta = 180^{o}$), the flow pattern sequence was similar to that shown in Fig. 28. However, in the divergent case, the vortices appeared to be stronger at the end of the arc as would be predicted by theory.

At higher rotational speeds and with lighter viscosity fluids ($\nu = 0.65$ centistokes) the flow patterns in the partial arc test rig eventually broke down into turbulence. This is shown in the sequence of photos in Fig. 30, ($\beta = 100^{o}$, $\epsilon = 0.706$). In the first photo, laminar vortex flow conditions prevail. The vortices to the far right of the arc are just beginning to develop the characteristic waviness which marks the onset of higher modes of instability of the flow. When this waviness first develops, it has a uniform sinusoidal quality. As speed increases, however, the waviness becomes increasingly irregular, taking on the character of turbulence. The second photo in Fig. 30 shows the large scale irregular eddying that is characteristic of the breakdown of the regular vortex waves. One can note that this eddying is confined to the vicinity of the leading edge of the arc where clearance is largest and flow is least stable. As flow is swept into the increasingly tighter clearances of the converging partial arc, the eddying is damped out.

The third photo in the sequence shows the flow at still higher speed. The flow to the right now appears to contain fully-developed turbulence but the flow to the left still appears laminar.

In the fourth and final photo, the flow is turbulent throughout the arc.

A similar sequence of developing turbulence also occurs in diverging partial arcs except that in the diverging case, maximum clearance is at the end of the arc and the flow is least stable at this point. Developing turbulence in a diverging partial arc is shown in the sequence of photographs in Fig. 31. Geometrical conditions are $\beta = 180^{\circ}$ and $\epsilon = 0.706$. In the first photograph, flow is laminar with developed vortices. One can note that the vortices appear stronger to the left (near exit of arc). In the second photo, eddying has developed near the exit of the arc. In the third photograph, flow is turbulent everywhere in the arc.

Prediction and Measurement of Transition Speeds in Partial-Arc Films

Theoretical prediction of the point of onset of vortices in a partial-arc bearing can be obtained by applying DiPrima's analysis of the stability of Couette flow with a circumferential pressure gradient (Ref. 4) to determine the local stability of velocity profiles within the partial arc. The procedure for doing this is described in Appendix B. Generally speaking, flow within a non-concentric partial arc will be least stable to development of vortices at the point where clearance is a maximum.

In the partial-arc studies at MTI, experimental runs were made with the arcs in three positions: 1) with the arc fully convergent ($\beta = 100^{\circ}$), 2) with the arc partially convergent and partially divergent ($\beta = 135^{\circ}$), and 3) with the arc fully divergent ($\beta = 180^{\circ}$). In the first two cases, the flow was least stable to vortices at the entrance to the arc while in the last case, flow was least stable at the exit.

Theoretical curves showing the transition speeds for onset of vortices at the least stable points in the partial arcs are drawn in Fig. 32. For the calculation of these curves, the pressure profiles within the partial arcs were determined by means of an analysis by P. C. Warner (Ref. 15). In the case of fully convergent and fully divergent arcs, the theoretical transition speeds were so very nearly the same that they are represented by one curve.

Experimental data from the partial-arc studies are compared with the theoretical curves in Fig. 32. In general, it was very difficult to determine the point of onset of vortices visually. This can be appreciated by consideration of the photos in Fig. 28. In this figure, the condition shown in photo (b) was taken to be the point of onset of vortices. For other geometries, the same criteria was applied. That is, the transition speed was judged to be that point where vortices became about as strongly pronounced as they are in photo (b) of Fig. 28. Obviously, it was difficult to be completely objective in one's judgement and the experimental points shown in Fig. 32 should be considered to involve considerable uncertainty.

The experimental points in Fig. 32 are in fairly good agreement with theory. One should note that the onset of vortices in the fully divergent arc occurred at higher speed than in the fully convergent case. This may be due to inertia effects in the flow. In general, however, DiPrima's analysis seems to provide a fairly accurate prediction of transition speed for partial arc geometries. In fact, DiPrima's analysis appears to be significantly more accurate in the case of partial arcs than in the case of full 360 degree cylinders. Other evidence of the validity of DiPrima's analysis for the case of partial arcs, was obtained previously in a study of the performance of an actual partial arc bearing running under both laminar and superlaminar flow conditions (Ref. 16).

Development of turbulence in partial arc bearings seemed always to occur at about the point where the Reynolds number based on local clearance, $\frac{V_1 d}{\nu}$, obtained a value of approximately 1000. This is in agreement with observations made previously (Ref. 9) for flow between full 360 degree cylinders.

The experiments show quite conclusively that fully developed vortex flow will occur in partial arcs. Also, the experiments provide evidence that DiPrima's analysis of flow stability can be applied with good quantitative accuracy to predict the point of onset of vortices.

INVESTIGATION OF THE FEASIBILITY OF USING THE ELECTROCHEMILUMINESCENT FLOW VISUALIZATION TECHNIQUE FOR STUDYING BEARING FLOW

A novel flow visualization process has been investigated by Howland, Pitts and Gesteland (Ref. 10). This technique, known as electrochemiluminescence, works in the following way. The surface over which flow patterns are to be studied is immersed in a chemiluminescent solution*. A small potential difference is maintained between this surface and a reference electrode located elsewhere in the solution. The surface to be studied should be the anode (positive electrode). Flow of electric current stimulates the emission of a chemiluminescent glow right at the anodic surface. The intensity of this glow depends on the rate of mass transfer of fresh reactants into the boundary layer along the anodic surface. Thus, if the boundary layer is turbulent, the turbulent eddies show up as variations in the intensity of the chemiluminescence. Test photographs made by Howland, Pitts and Gesteland (Ref. 10) show that this flow visualization technique revealed boundary layer flow patterns with excellent clarity.

The electrochemiluminescent flow visualization technique has two characteristics which make it appear promising for studying flow patterns in bearings. The first is that this technique does not interfere in any way with the flow. This is of obvious importance in bearings where the clearances are very small and where visual techniques involving suspended particles would be impossible to use. The second advantageous characteristic of the electrochemiluminescent technique is that the glow is apparently confined to an extremely thin layer next to the anode surface. Howland and co-workers have conjectured that at certain alkalinity levels of the solution, the glow may take place entirely within a few wavelengths of the surface. This also makes this visualization technique ideally suited for very close clearances flows.

Because of the potential usefulness of the electrochemiluminescent process for studying turbulence and vortex flow in bearings, some time was spent exploring the feasibility of using this technique in the present studies of superlaminar flow. The test apparatus used for these exploratory studies is shown in Fig. 33. The rig consists of a beaker in which there is a 5/8 inch I.D. glass sleeve. A 1/2 inch platinum-coated shaft, rotated by a variable speed drive, extends into the glass sleeve from above. This platinum-covered shaft is overcoated with an insulating layer of epoxy except for a one inch long section within the glass sleeve. The platinum shaft is electrically connected to the positive terminal of a low-voltage d-c power supply. A platinum cathode is contained in the beaker. The entire beaker is filled with an electrochemiluminescent solution consisting mainly of water as solvent with KCL as a supporting electrolyte and Luminol as the chemiluminescent substance. When a potential difference on the order of two volts is maintained

---

*There are a number of different chemiluminescent solutions which can be used. The chemical compositions of some of these are given in Ref. 10.

between the platinum-plated shaft and the platinum electrode, a blue glow occurs in the film immediately adjacent to the surface of the platinum shaft within the glass sleeve (the part of the shaft not coated with epoxy). The glow pattern should reveal the onset of a Taylor vortex flow pattern or the onset of turbulence since these flow patterns will result in local variations in liquid mass transport at the shaft surface.

The use of platinum or platinum-covered shafts in the electrochemiluminescent technique is necessary because other materials will electrolytically corrode in the chemiluminescent solution. Originally, the shafts were copper with platinum plating. However, these were not successfull because pinhole imperfections in the plating allowed the solution to attack the copper underneath the plating. Ultimately, the shaft was covered with platinum foil of a few mils thickness. This worked satisfactorily. The fact that platinum surfaces are required is a serious disadvantage to the technique not only because of their cost but also because of the questionable machinability of platinum. Other difficulties associated with the technique are:

1. The electrolytic reaction that occurred caused emission of gas bubbles at the anodic surface. This was minimized by thoroughly degassing the solution but it always remained somewhat of a problem.

2. The glow emitted at the surface was very faint, prohibiting very rapid exposures. Since the time scale of turbulent fluctuations should be quite rapid with a rapidly revolving shaft, it may not be possible to photograph the turbulent flow field.

3. If the radial clearance between the shaft and the glass sleeve were to approach bearing clearances, then the resistance of the electrical path between the shaft surface within the sleeve and the cathode outside could become very large. Possibly, this would prohibit development of a glow pattern within the glass sleeve. This might be overcome by using a semi-transparent metallic film on the inside of the glass sleeve as the cathode surface.

4. A final possible difficulty associated with using the electrochemiluminescent technique for visualization of bearing flows is that the supply of fresh reactant to the thin fluid film in the bearing might be inadequate to sustain the glow.

In spite of the difficulties mentioned above, a vortex flow pattern was made visible by electrochemiluminescence. This vortex flow pattern is shown in Fig. 34. Between each pair of dark horizontal lines is contained a pair of vortices. The dark lines mark regions where flow is coming out from the surface of the inner shaft: this flow being depleted of fresh reactants where it leaves the surface.

The fact that a vortex flow pattern could be made visible by electrochemiluminescence is evidence that this technique could be feasible for study of bearing flow patterns. However, due to the above-mentioned difficulties

associated with the technique, it appears that extensive development work would be required to make it an effective investigatory tool. Consequently, study of the technique was stopped. In view of the novel advantages possessed by the technique, however, it should be given consideration whenever future, difficult flow visualization problems are encountered.

CONCLUSIONS

Transition Speed for Onset of Vortices

Flow between non-concentric rotating cylinders

The critical speed at which vortices first develop in the flow between a rotating inner cylinder and a non-concentric stationary outer cylinder increases with eccentricity ratio of the cylinders. The relationship between transition speed and eccentricity ratio measured for $C/R_1 = 0.0104$ was found to be significantly different from that measured for $C/R_1 = 0.099$. It is believed that the difference was due primarily to the influence of flow inertia effects at the larger clearance ratio. Evidence obtained from pressure profile measurements indicate that at the lower clearance ratio, inertia effects are no longer significant with respect to the development of vortices. Therefore, it is believed that the data for transition speed vs. eccentricity ratio obtained at $C/R_1 = 0.0104$ (Figure 8) is valid for lower clearance ratios, such as are characteristic of bearings, in spite of the fact that this data is not in agreement with the approximate analysis of DiPrima.

Flow between rotating inner cylinder and outer partial arc

Transition speeds for onset of vortices in the film between a partial-arc outer cylinder and rotating inner cylinder were determined visually and, as a result, are not as precise as those determined for full rotating cylinders by means of torque measurements. Within the uncertainty of the measurements, however, it appears that DiPrima's theoretical prediction of the stability of Couette flow with a circumferential pressure gradient applies with quite good accuracy to partial arcs. Other evidence in support of this was obtained in a previous experimental study of an actual partial-arc bearing (Ref. 16).

The recommended procedure for determining transition speeds for onset of vortices in partial arcs by means of DiPrima's analysis is described in Appendix B.

Frictional Drag Between Rotating Cylinders in Superlaminar Flow Regime

Vortex flow regime

At speeds just above Taylor transition speed, ($T_c < T < 2T_c$) the torque between non-concentric cylinders can be predicted with quite good accuracy by means of DiPrima's analysis (Ref. 1) provided one uses the measured values of Taylor transition number in the calculations rather than the theoretical value. The exact procedure for calculating torques in this way is described in Appendix A.

Turbulent-vortex flow regime

For speeds well above Taylor transition speed ($T > 2T_c$), when turbulence as well as vortices are present in the flow, the friction factor λ for flow between concentric cylinders is predicted quite accurately by means of the empirical formulae suggested by Wendt (Ref. 13).

$$\lambda = 0.46 \left[\frac{(R_2-R_1)R_2}{R_1^2}\right]^{\frac{1}{4}} (N_{Re})^{-0.5} \qquad \left(80\sqrt{\frac{R_1}{C}} < N_{Re} < 10^4\right) \qquad (10)$$

$$\lambda = 0.073 \left[\frac{(R_2-R_1)R_2}{R_1^2}\right]^{\frac{1}{4}} (N_{Re})^{-0.3} \qquad (10^4 < N_{Re} < 10^5) \qquad (11)$$

For eccentric cylinders of large length to diameter ratio (L/D > 2.0) and with complete fluid film it is recommended that the friction factor λ be calculated by means of Wendt's formulae and corrected for the effect of eccentricity by means of the dashed curve shown in Fig. 16. For eccentric cylinders of shorter length to diameter ratio (L/D < 2.0) or with incomplete fluid films the above procedure will yield conservatively high values of torque.

Pressure Profiles in Superlaminar Flow Between Non-Concentric Rotating Cylinders

Vortex flow regime

The onset of vortices in the flow between non-concentric rotating cylinders results in a change in both the shape and magnitude of the pressure profile around the cylinders. Of these, the change in the magnitude of the pressure profile is the most important. For speeds just above Taylor transition speed ($T_c < T < 2T_c$) the pressure profiles are predicted with good accuracy by means of DiPrima's analysis (Ref. 1) if one uses measured values for T_c rather than theoretical values. The procedure for calculating the pressure profile is described in Appendix A.

Turbulent-vortex flow regime

In the fully-developed turbulent regime ($N_{Re} > 2500$), pressure profiles can be calculated by means of the turbulent lubrication theory of Ng and Pan (Ref. 3). This theory agreed well with pressure measurements made in the present experiments for Reynolds numbers above 2400.

APPENDIX A

CALCULATION OF FLUID FRICTION AND PRESSURE PROFILES FOR TAYLOR VORTEX FLOW BETWEEN NON-CONCENTRIC ROTATING CYLINDERS

R. C. DiPrima (Ref. 1) has obtained the following theoretical relationships for flow between concentric cylinders in the vortex regime at speeds just above Taylor critical speed.

$$\frac{V_m}{V_1} = 1/2 + Q/6 + \left(1 - \frac{T_c(Q)}{T}\right) F(Q)\ G(Q) \qquad \text{A-1}$$

$$-\frac{\tau'}{\mu V_1/d} = 1 - Q + \left(1 - \frac{T_c(Q)}{T}\right) H(Q) \qquad \text{A-2}$$

where

V_m = mean circumferential flow velocity due to sum of Couette flow and pressure flow

τ' = local shear stress at surface of inner cylinder

$Q = 3\ V_p/V_c = 3\left(-\frac{d^2}{12\mu R_1}\ \frac{\partial P}{\partial \theta}\right)\ \frac{2}{V_1}$

V_p = mean circumferential velocity due to pressure gradient

V_c = mean circumferential velocity due to rotation

τ' = local shear stress at surface of inner cylinder

V_1 = surface velocity inner cylinder

R_1 = radius inner cylinder

R_2 = radius outer cylinder

μ = fluid velocity

T = local Taylor number $= 4\left(\frac{V_1 d}{\nu}\right)^2\ \frac{d}{R_1 + R_2}$

d = local radial clearance between inner and outer cylinder = $C\ (1 + \epsilon \cos \theta)$

$T_c(Q)$= local transition value of Taylor number for onset of vortices $T_c(Q)$ is a tabulated function of Q

$F(Q)$, $G(Q)$, $H(Q)$ Tabulated functions of Q.

Relations A-1 and A-2 are derived for the case where both clearance and pressure gradient do not vary circumferentially. In the case of non-concentric rotating cylinders, both clearance and pressure gradient do vary around the cylinders. Q, therefore, varies circumferentially. To obtain an approximate calculation of the effect of vortex motion on shear stress and pressure gradient in the flow between non-concentric cylinders, one can apply relations A-1 and A-2 locally at each circumferential point using the appropriate local values of Q and sum these local contributions. The procedure is as follows:

First, using laminar flow theory (e.g., Sommerfeld theory), one obtains a solution for $Q(\theta)$. One next determines $T_c(Q)$ at each circumferential position. If $T_c < T$ at any point, then it is assumed that vortices will be present at those points and equations A-1 and A-2 will apply. If $T_c > T$, then flow is locally laminar and the following equations would apply locally.

$$V_m/V_1 = 1/2 + Q/6 \qquad \text{A-3}$$

$$-\frac{\tau'}{\mu V_1/d} = 1 - Q \qquad \text{A-4}$$

The presence of vortices anywhere in the flow alters the values of $Q(\theta)$ everywhere and also changes the value of $V_m(\theta)/V_1$. Let us denote the solution for $V_m(\theta)/V_1$ obtained from laminar theory as $(V_m/V_1)_L$. By requirement of continuity of flow, all permissible solutions for $V_m(\theta)/V_1$ must be of the form

$$\frac{V_m(\theta)}{V_1} = (V_m/V_1)_L + \frac{K}{1 + \varepsilon \cos \theta} \qquad \text{A-5}$$

where K is an arbitrary constant.

Substituting for V_m/V_1 in A-1 and A-3 by means of A-5, we obtain

$$(V_m/V_1)_L + \frac{K}{1 + \varepsilon \cos \theta} = 1/2 + Q/6 + \left(1 - \frac{T_c(Q)}{T}\right) F(Q)\, G(Q);\quad T_c < T \qquad \text{A-6}$$

$$(V_m/V_1)_L + \frac{K}{1 + \varepsilon \cos \theta} = 1/2 + Q/6; \qquad T_c > T \qquad \text{A-7}$$

Given a value of K, one can solve equations A-6 and A-7 for $Q(\theta)$. Having obtained $Q(\theta)$, $\frac{\partial P}{\partial \theta}$ can be calculated

$$\frac{\partial P}{\partial \theta} = -\frac{2\mu R_1 V_1}{C^2(1 + \varepsilon \cos \theta)^2}\, Q(\theta) \qquad \text{A-8}$$

$\frac{\partial P}{\partial \theta}$ has the condition imposed upon that

$$\int_0^{2\pi} \frac{\partial P}{\partial \theta}\, d\theta = 0 \qquad \text{A-9}$$

To find the proper value of the constant K, we follow a trial and error process. That is, we first make a reasonable guess for K (K is always positive), and then calculate $Q(\theta)$ and $\frac{\partial P}{\partial \theta}$ from A-6, A-7 and A-8 respectively. We then test to see if the condition A-9 is satisfied. If it is, then our guess for K is the correct one. If the integral in A-9 is greater than zero, our guess for K was too small and should be increased. Conversely, if the integral is less than zero, our guess for K was too large and should be reduced.

When the proper values for K, $A(\theta)$ and $\frac{\partial P}{\partial \theta}$ are determined, then the local shear stress τ' can be calculated from A-2 and A-4 and summed to obtain the total frictional drag on the inner cylinder.

Calculation of τ' and $\partial P/\partial \theta$ by the above procedure is obviously a tedious process. A computer program suitable for running on the GE 205 digital computer has been written to perform the calculations. The program assumes the Sommerfeld solution in the laminar flow range and is, therefore, applicable only to cylinders of reasonably large length-to-diameter ratios and with complete fluid films. The functions $F(Q)$ $G(Q)$, $H(Q)$ and $T_c(Q)$ required for computation are given in tabular form below for the case of outer cylinder stationary.

TABLE OF FUNCTIONS OF Q

Q	F(Q) G(Q)	H(Q)	$T_c(Q)$
-3.665	0.341	0.312	71785.6
-3.65	0.342	0.423	70784.6
-3.60	0.335	0.638	68000.0
-3.50	0.319	0.784	62867.0
-3.25	0.302	0.929	51257.0
-3.00	0.291	0.978	40943.0
-2.6	0.273	1.17	26500.0
-2.2	0.232	1.435	16250.0
-2.0	0.185	1.570	12540.0
-1.8	0.152	1.585	10000.0
-1.6	0.125	1.570	8200.0
-1.2	0.085	1.525	6150.0
-0.8	0.060	1.480	4820.0
-0.4	.039	1.45	3960.0
0	.021	1.433	3390.0
0.4	-0.0055	1.430	2930.0
0.8	-0.01	1.436	2570.0
1.2	-0.026	1.453	2300.0
1.6	-0.042	1.477	2070.0
2.0	-0.058	1.51	1880.0
2.4	-0.0735	1.548	1700.0
2.8	-0.089	1.592	1505.0
21.0	-0.873	4.926	149.0
46.0	-0.873	4.926	149.0

APPENDIX B

CALCULATION OF TRANSITION SPEED FOR ONSET OF VORTICES IN FLUID FILM BETWEEN A ROTATING INNER CYLINDER AND AN OUTER PARTIAL ARC

DiPrima (Ref. 4) has calculated the transition value of Taylor number, T_c, for onset of vortices in a Couette flow with a circumferential pressure gradient. The transition Taylor number is given as a tabulated function of the flow parameter Q where

$$Q = 3\ V_P/V_c = 3 \left(\frac{-d^2}{12\mu R_1} \quad \frac{\partial P}{\partial \theta} \right) \quad \frac{2}{V_1} \qquad \text{B-1}$$

To determine the transition speed for onset of vortices in the partial-arc fluid film, one first calculates the pressure gradient (and hence Q) everywhere in the fluid film. One next determines the local transition Taylor numbers for every point in the fluid film from the tabulated values of $T_c(Q)$. Theoretically, onset of vortices should occur in the partial-arc fluid film when the value of the local Taylor number

$$T = 4 \left(\frac{V_1 d}{\nu}\right) \frac{d}{R_1 + R_2} \qquad \text{B-2}$$

exceeds the value T_c (Q) at any point within the partial arc film. One should note that this criterion for stability of flow within a partial arc does not take account of the stabilizing influence of any axial flows that may be present.

Tabular values of T_c (Q) are presented in the preceding appendix (Appendix A).

REFERENCES

1. DiPrima, R.C., "Viscous Flow between Rotating Concentric Cylinders with a Circumferential Pressure Gradient at Speeds above Critical," ASLE Transactions 7, pp 333-341, Oct, 1964.
2. Taylor, G.I., "Stability of a Viscous Liquid Contained between Two Rotating Cylinders," Philosophical Transactions, A, Vol. 223, 1023, pp 289-343.
3. Ng, C.W., and Pan, C.H.T., "A Linearized Turbulent Lubrication Theory," ASME Paper No. 64-Lub-29, presented at the ASME-ASLE International Conference, Washington, D.C., Oct. 13-16, 1964.
4. DiPrima, R.C., "The Stability of a Viscous Flow between Rotating Cylinders with a Pressure Gradient Acting Round the Cylinders," J. Fluid Mech. 6, 462-468 (1959).
5. Hughes, T.H., and Reid, W.H., "The Effect of a Transverse Pressure Gradient on the Stability of Couette Flow," ZAMP 15, pp 573-581 (1964).
6. Kurzweg, U.H., "A Note on the Stability of Generalized Couette Flow," ZAMP 14, pp 380-383 (1963).
7. Meister, B., "Das Taylor-Deansche Stabilitatsproblem für beliebige Spaltbreiten," ZAMP 13, pp 83-91, (1962).
8. DiPrima, R.C., "A Note on the Stability of Flow in Loaded Journal Bearings" ASLE Transactions, 6, pp 249-253 (1963).
9. Vohr, J.H., "Analysis of Turbulent Lubrication, Volume 2, An Experimental Study of Vortex Flow and Turbulence in Concentric and Eccentric Annuli" (Vol. 2 of Final Report on NASA Contract NASw-771), May 20, 1964, NASACR-CR-54034, MTI 64TR20.
10. Howland, B., Pitts, W.H., Gesteland, R.C., "Use of Electrochemiluminescence for Visualizing Fields of Flow," MIT Research Laboratory of Electronics Technical Report 404, September 21, 1962.
11. Pinkus, O., and Sternlicht, B., "Theory of Hydrodynamic Lubrication," McGraw-Hill Book Co., Inc., 1961, pp 352-353.
12. Sommerfeld, A. "Zur Hydrodynamischen Theory der Schmiermittelreibung," Z. Math. u. Physik, Vol. 50, page 97, (1904).
13. Wendt, F., "Turbulente Stromungen Zwischen Zwei Rotierenden Konoxialen Zylindern," Ingenieur-Archiv 4, 1933, pp 577-595.
14. Smith, M.I., and Fuller, D.D., "Journal Bearing Operation at Super-Laminar Speeds," Trans. ASME Vol. 78, 1956, p 469.
15. Warner P.C., "Static and Dynamic Properties of Partial Journal Bearings," Journal of Basic Engineering, Trans. ASME, Series D, Vol. 85, 1963, p 247.
16. Orcutt, F.K., "Investigation of a Partial Arc Pad Bearing in the Super-Laminar Flow Regime," Journal of Basic Engineering, Vol. 87, Series D, No.1, March 1965, pp 145-152.

17. DiPrima, R.C., "The Stability of a Viscous Fluid between Rotating Cylinders with an Axial Flow." Journal of Fluid Mechanics Vol. 9, Part 4, pp 621-631, 1960.

18. Donnelly, R.J., and Fultz, D., "Experiments on the Stability of Spiral Flow between Rotating Cylinders," Proc. Nat. Acad., Sci. 46, 1960, pp 1150-1154.

19. Snyder, H.A., "Experiments on the Stability of Spiral Flow at Low Axial Reynolds Numbers, "Proceedings of the Royal Society of London, Series A, Vol. 265, 1962, pp 198-214.

20. Krueger, E.R., and Di Prima, R.C., "On the Stability of Spiral Flow between Rotating Cylinders," MRC Technical Summary Report # 430, Mathematics Research Center, United States Army, The University of Wisconsin, 1963.

21. Orcutt, F.K., "Analysis of Turbulent Lubrication. Vol. 1. The Static and Dynamic Properties of Journal Bearings in Laminar and Turbulent Regimes." Mechanical Technology Incorporated report no. MTI-64TR19. Final Report to NASA on contract NASw-771, May 1964.

SYMBOLS

C	radial clearance, inches
D	diameter of inner cylinder, inches
d	local fluid film clearance between inner and outer cylinders, inches
e	eccentricity of inner cylinder within outer cylinder, inches
$F(Q)$, $G(Q)$, $H(Q)$	tabulated functions of Q
G	torque, inch-pounds
G_L	theoretical laminar torque for rotating cylinders, inch-pounds
K	arbitrary constant
L	length of inner cylinder, inches
N_{Re}	Reynolds number, $V_1 C/\nu$
P	pressure, pounds/inch^2
P_{max}	peak fluid film pressure, pounds/inch^2
$(P_L)_{max}$	peak theoretical fluid film pressure assuming laminar flow, pounds/inch^2
Q	$3\ V_p/V_c$
R_1	radius of inner cylinder, inches
R_2	radius of outer cylinder, inches
T	Taylor number $4\left(\frac{V_1 C}{\nu}\right)^2 \frac{C}{R_1 + R_2}$
T_c	value of Taylor number at transition to vortex flow
υ	volume, inch^3
V	fluid film velocity in the circumferential direction, inch/second
V_1	surface velocity of inner cylinder, inches/second
$V_c = V_1/2$	mean circumferential flow velocity due to rotation, inches/second
V_m	mean circumferential flow velocity due to sum of Couette flow and pressure flow, inches/second
V_p	mean circumferential flow velocity due to pressure gradient, inches/second
y	coordinate normal to bearing surface, inches
β	angle between leading edge of partial arc and point of maximum clearance
ε	eccentricity ratio, e/c
θ	circumferential coordinate in direction of rotation
λ	friction factor, $2\tau/\rho V_1^2$
μ	absolute viscosity, pound-seconds/inch^2
ν	kinematic viscosity, inches/second^2
ρ	mass density, pound-seconds^2/inch^4
τ	mean surface shear stress on inner cylinder, pounds/inch^2
τ'	local shear stress at surface of inner cylinder, pounds/inch^2
Ω	rotational speed, radians/second

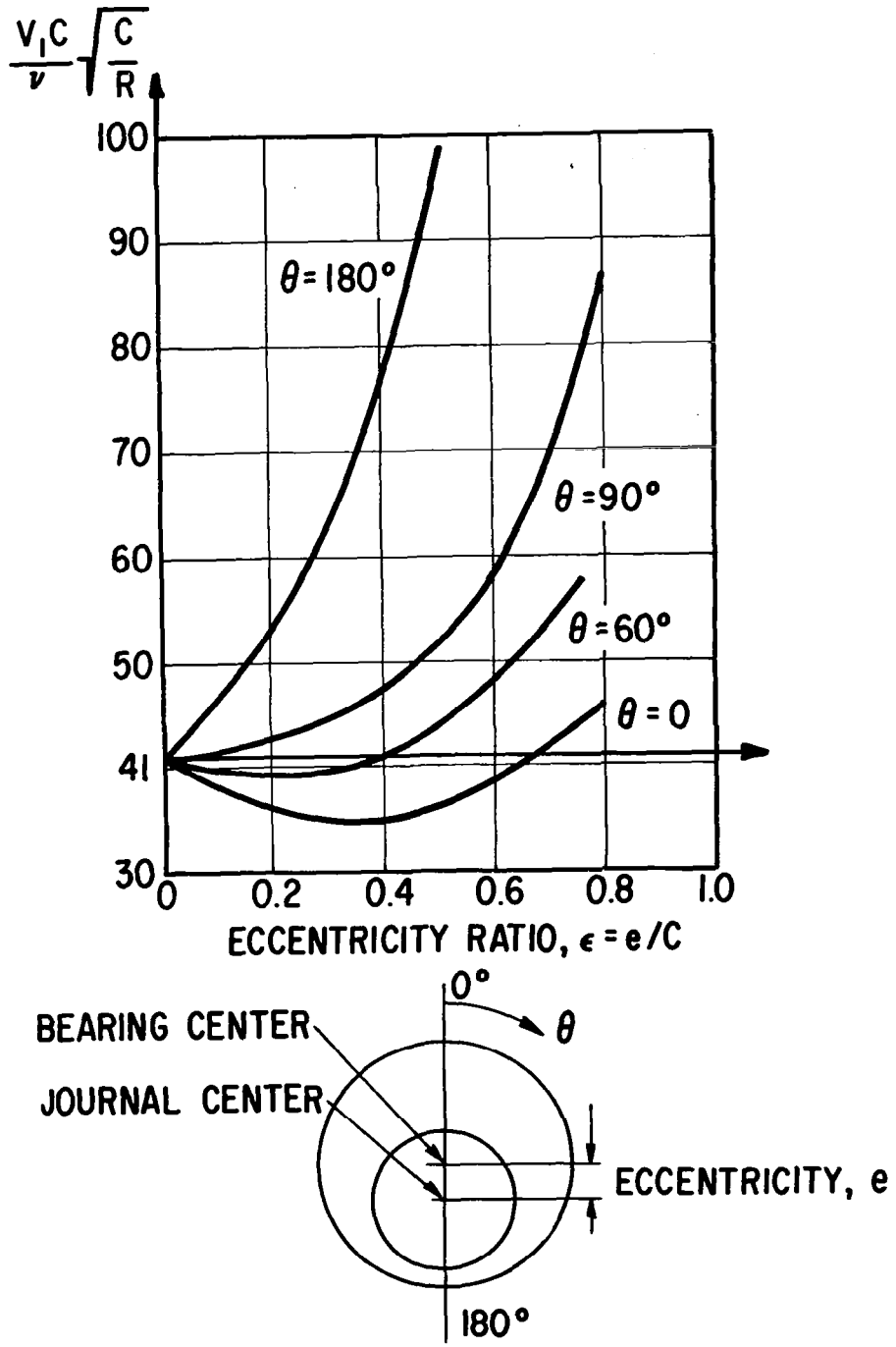

Figure 1. - Transition values of the parameter $V_1 C/\nu \sqrt{C/R_1}$ for onset of vortices in flow between non-concentric rotating cylinders at different circumferential positions.

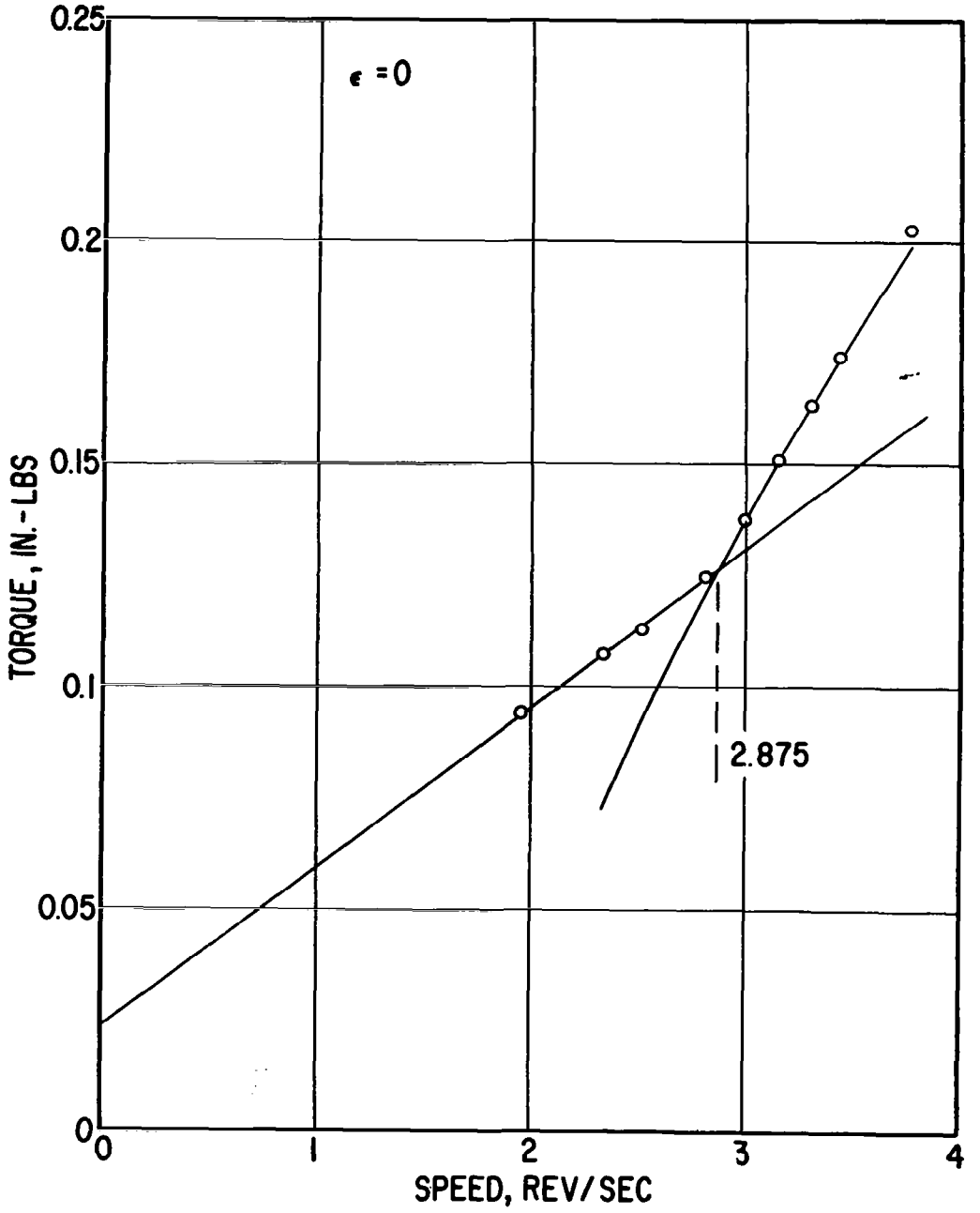

Figure 2. - Torque vs rotational speed curve showing onset of vortices; $C/R_1 = 0.0104$.

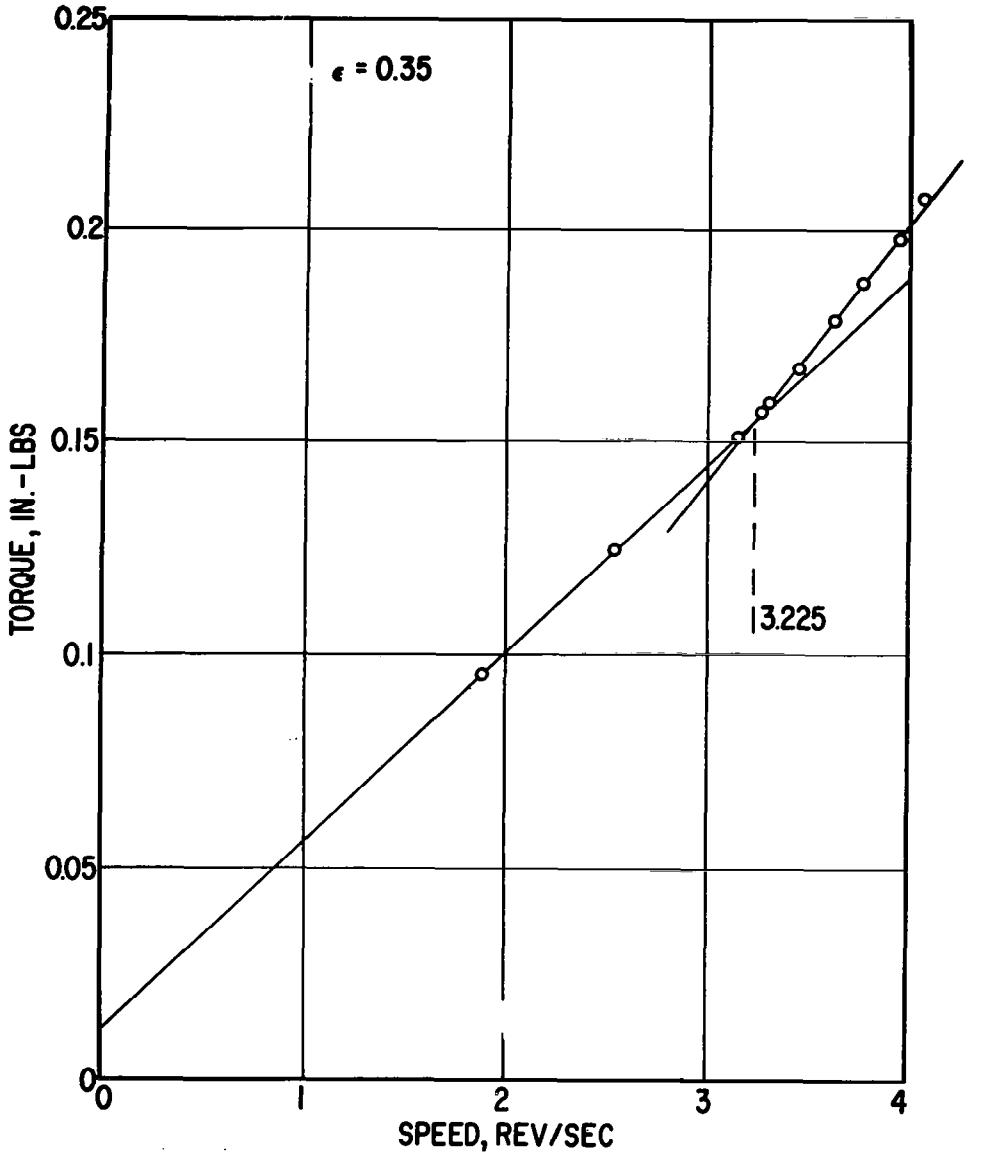

Figure 3. - Torque vs rotational speed curve showing onset of vortices; $C/R_1 = 0.0104$.

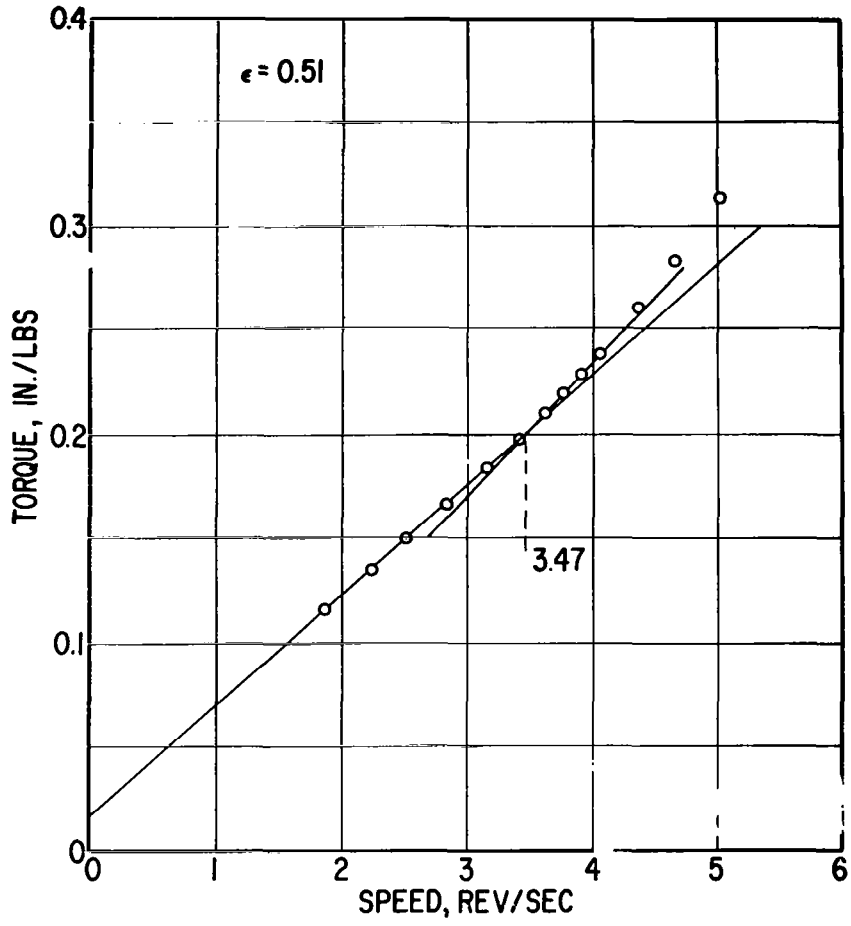

Figure 4. - Torque vs rotational speed curve showing onset of vortices; $C/R_1 = 0.0104$.

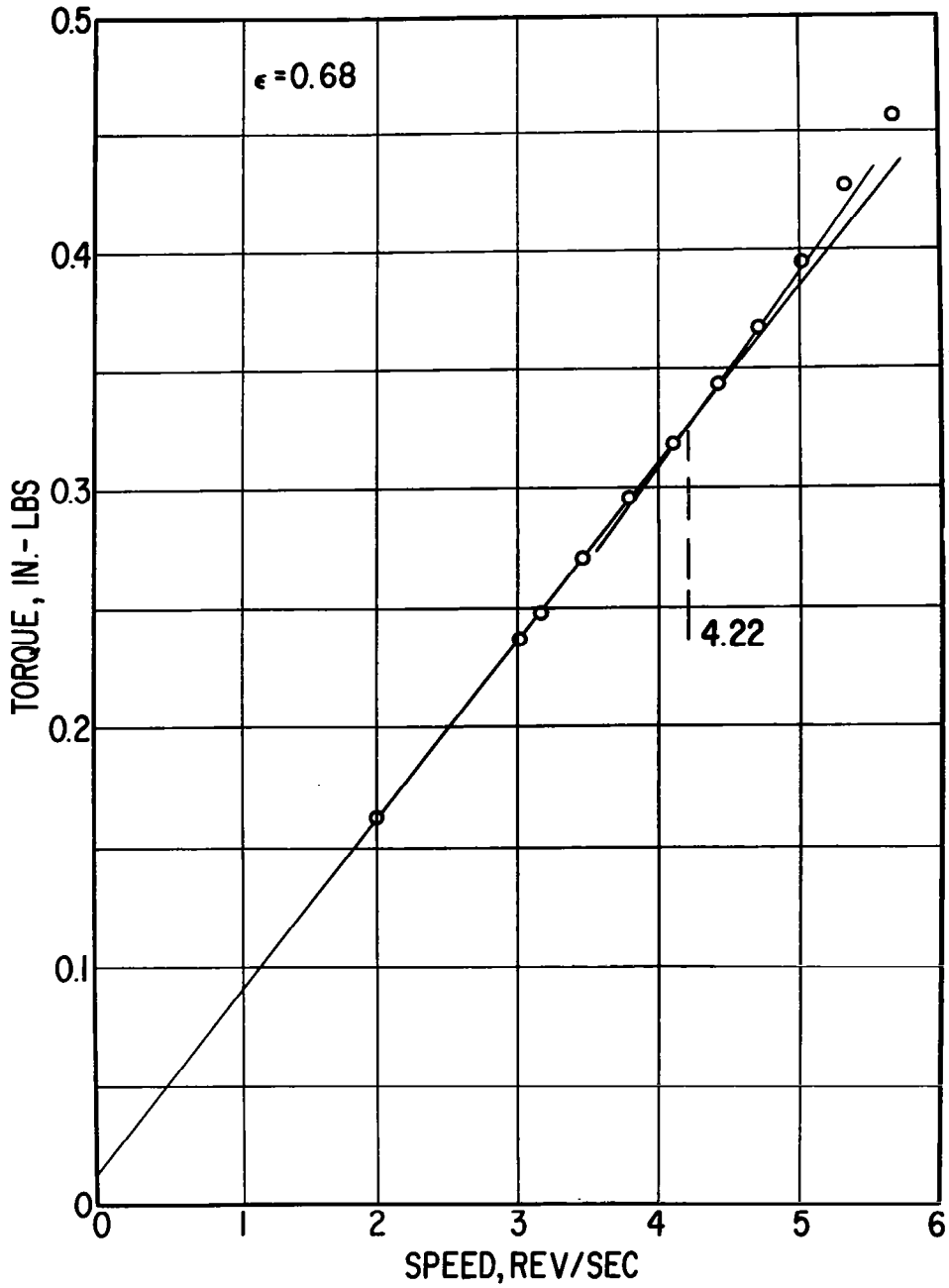

Figure 5. - Torque vs rotational speed curve showing onset of vortices; $C/R_1 = 0.0104$.

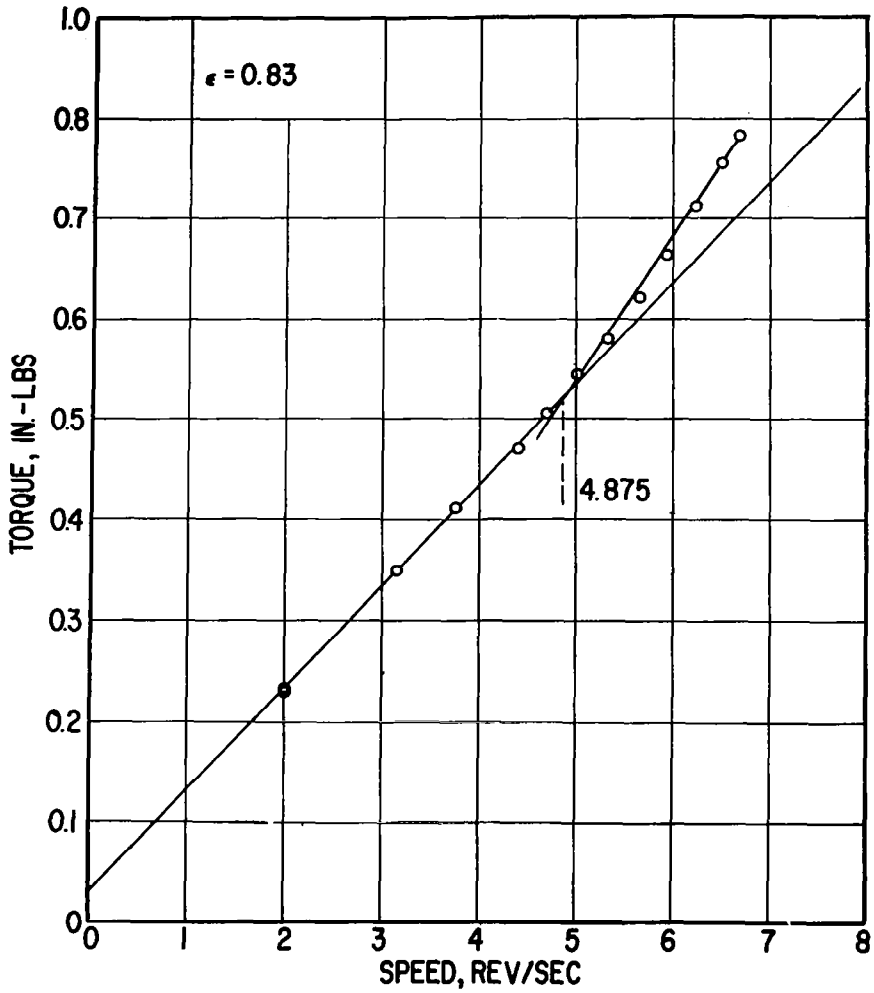

Figure 6. - Torque vs rotational speed curve showing onset of vortices; $C/R_1 = 0.0104$.

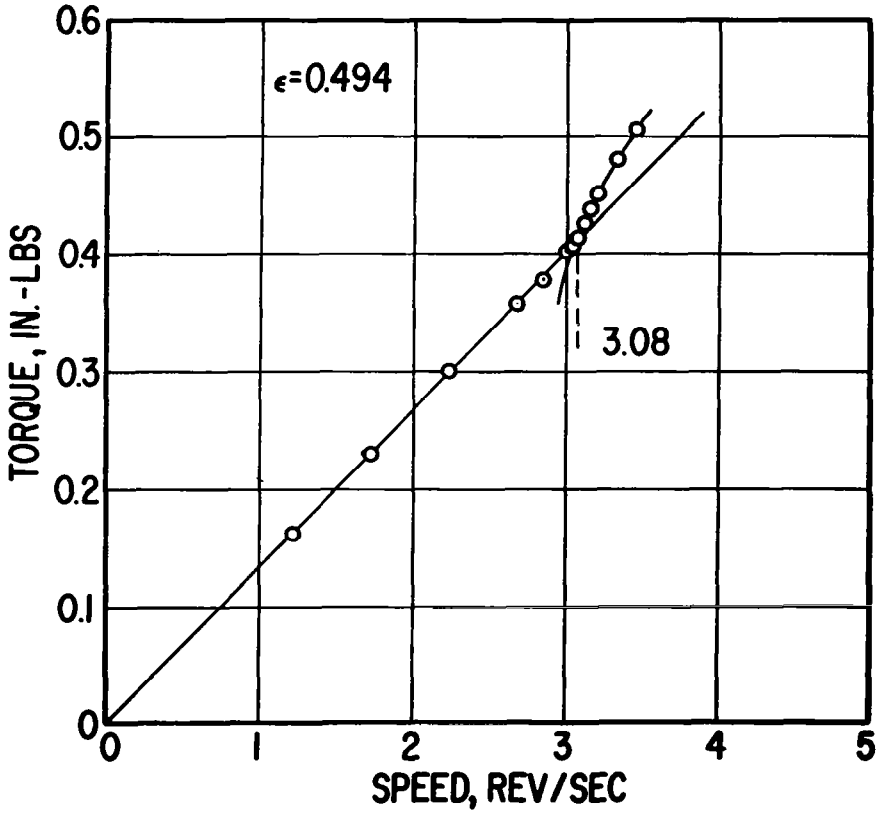

Figure 7. - Torque vs rotational speed curve showing onset of vortices; C/R_1 = 0.099 (ref. 9)

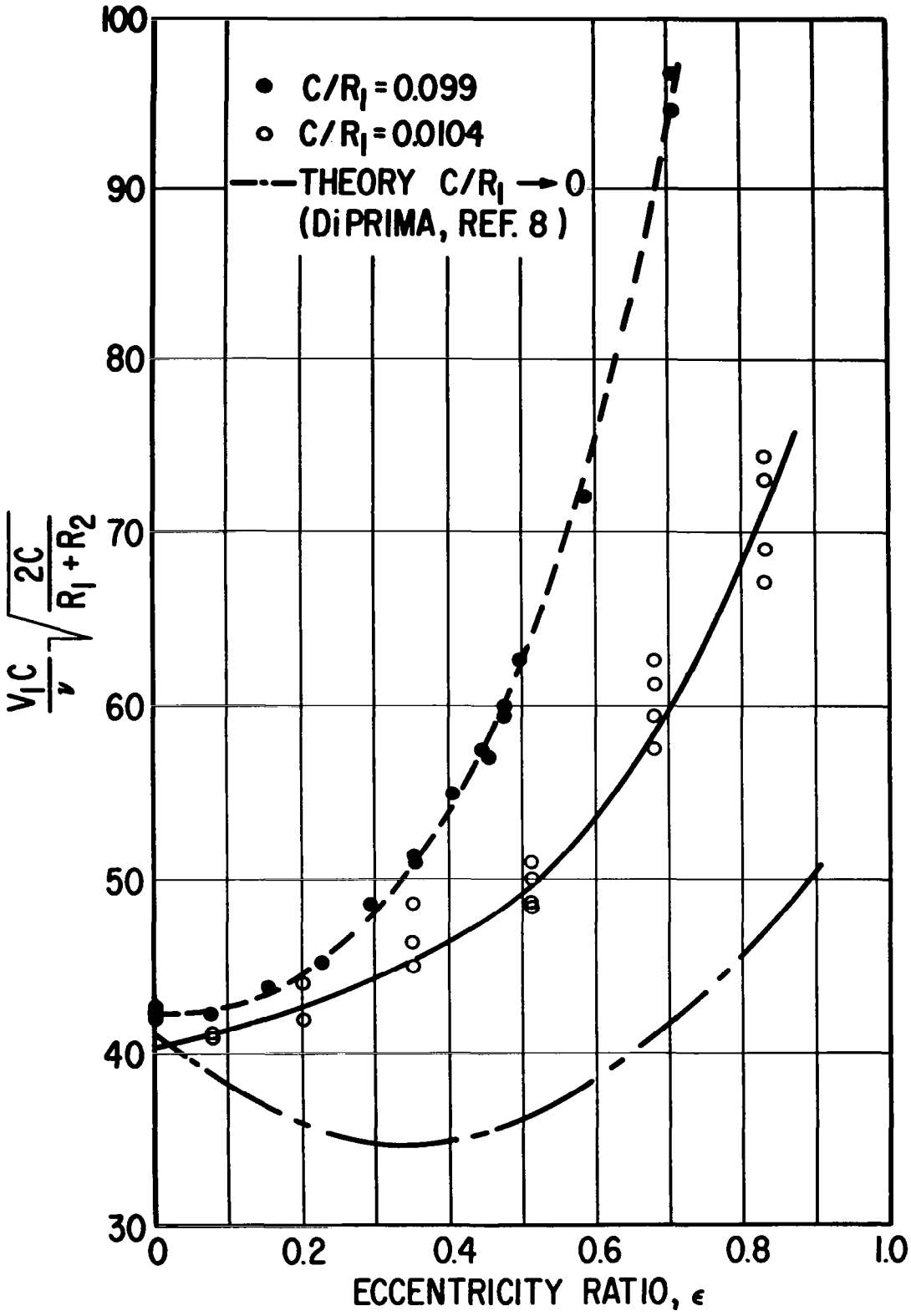

Figure 8. - Measured transition speeds for onset of vortices in flow between non-concentric cylinders.

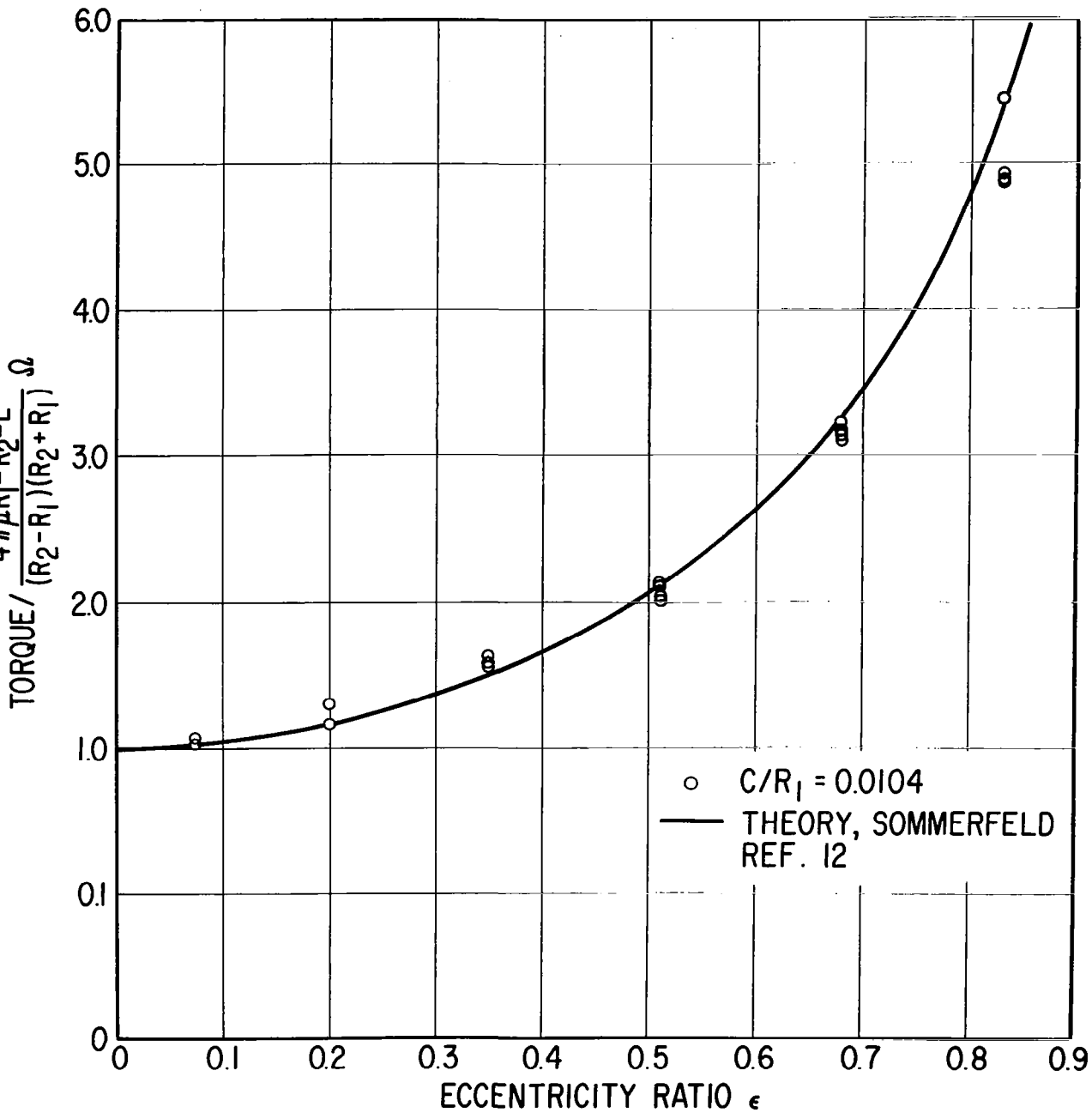

Figure 9. - Comparison of measured and theoretical values of torque for laminar flow between non-concentric cylinders; $C/R_1 = 0.0104$.

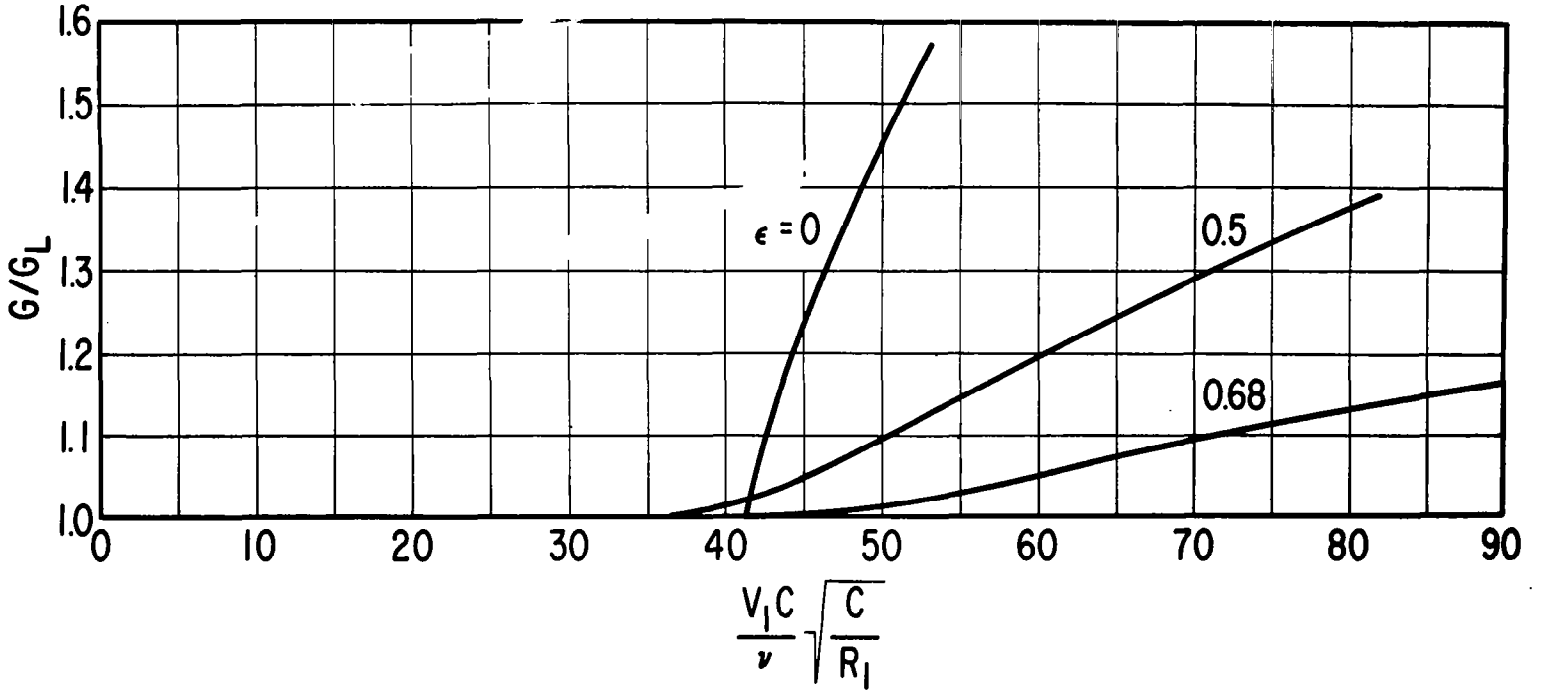

Figure 10. - Predicted ratio of torque, G, in vortex flow regime to torque, G_L, in laminar flow regime for cylinders at different eccentricity ratios.

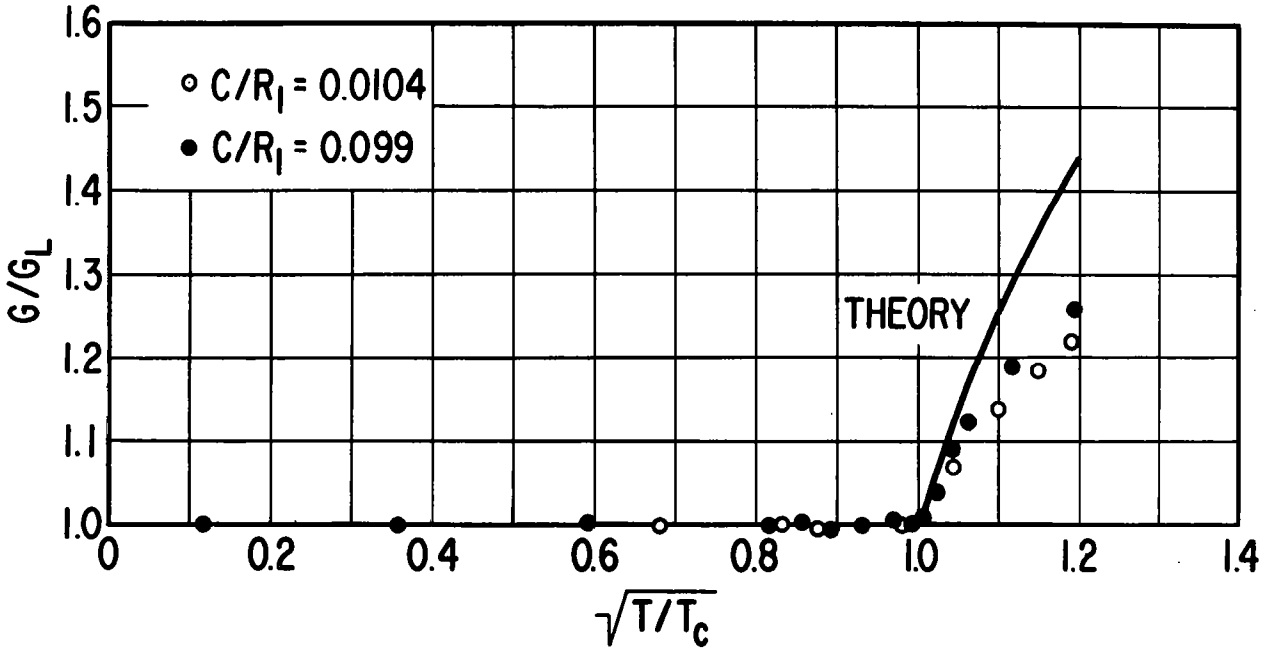

Figure 11. - Ratio of torque, G, in vortex flow regime to torque, G_L, in laminar flow regime; comparison of theory and experiment for concentric cylinders.

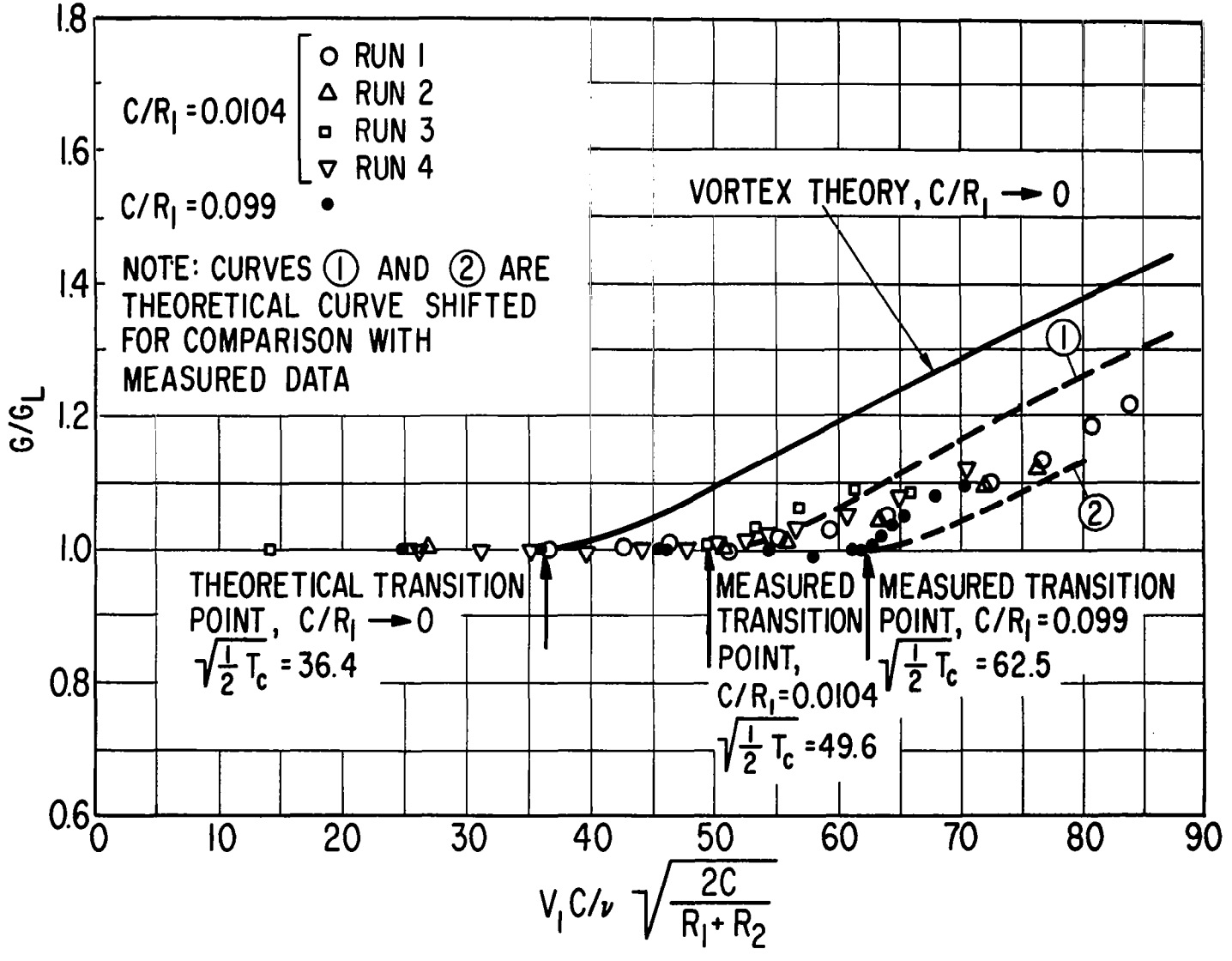

Figure 12. - Ratio of torque, G, in vortex flow regime to torque, G_L, in laminar flow regime; comparison of theory and experiment for cylinders at eccentricity ratio $\epsilon = 0.50$.

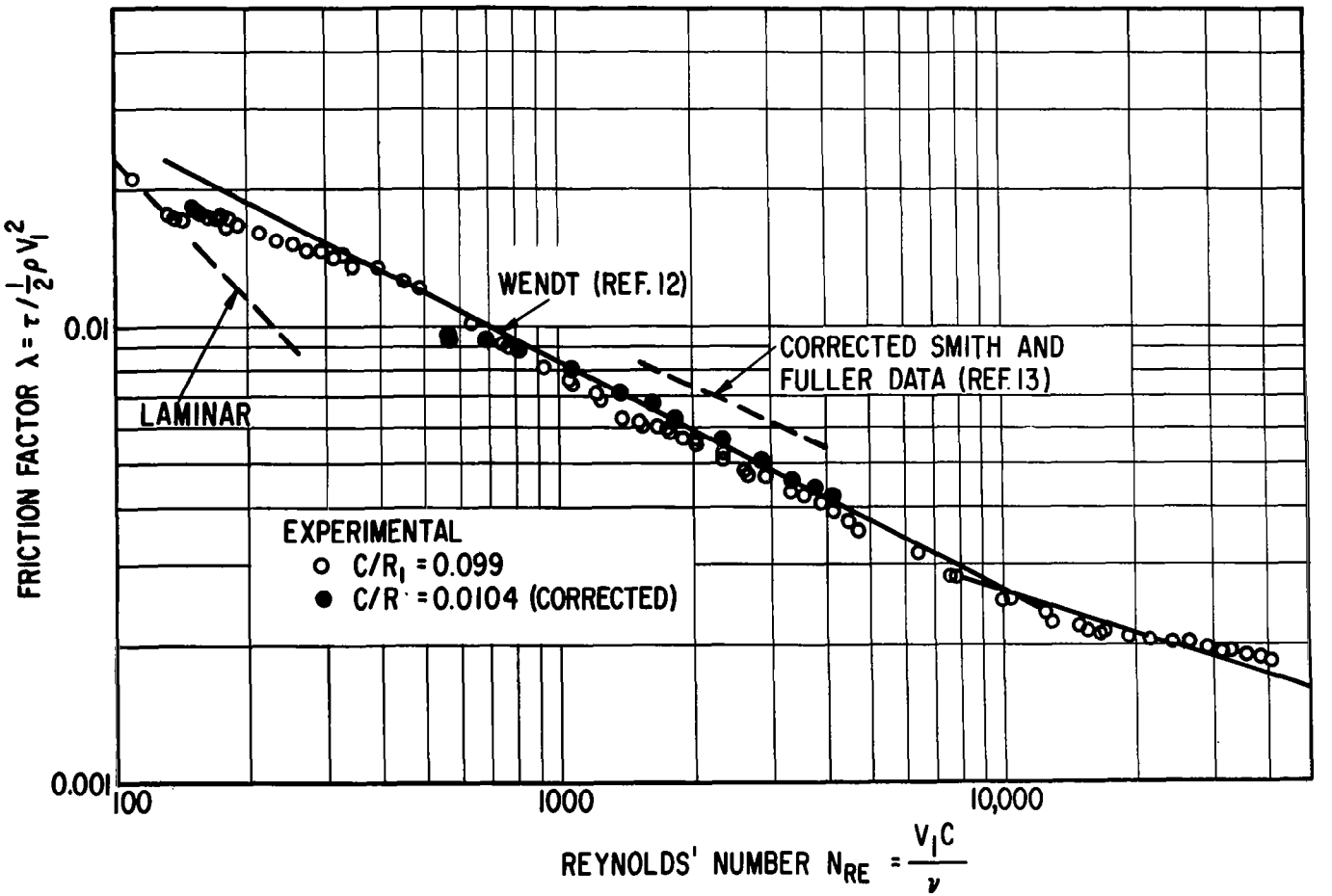

Figure 13. - Friction factor vs Reynolds number for flow between concentric rotating cylinders. (All data is corrected to a clearance ratio of 0.099.)

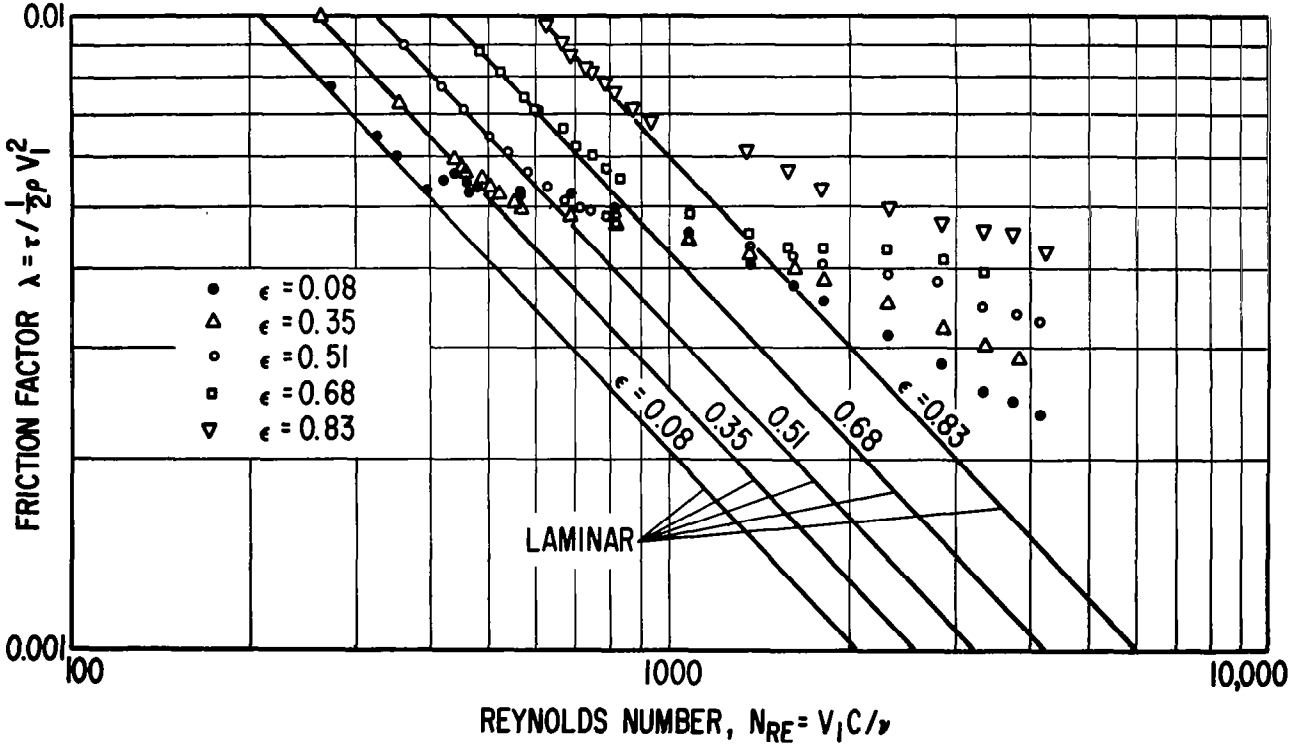

Figure 14. - Friction factor vs Reynolds number for flow between rotating cylinders at various eccentricity ratios; $C/R_1 = 0.0104$.

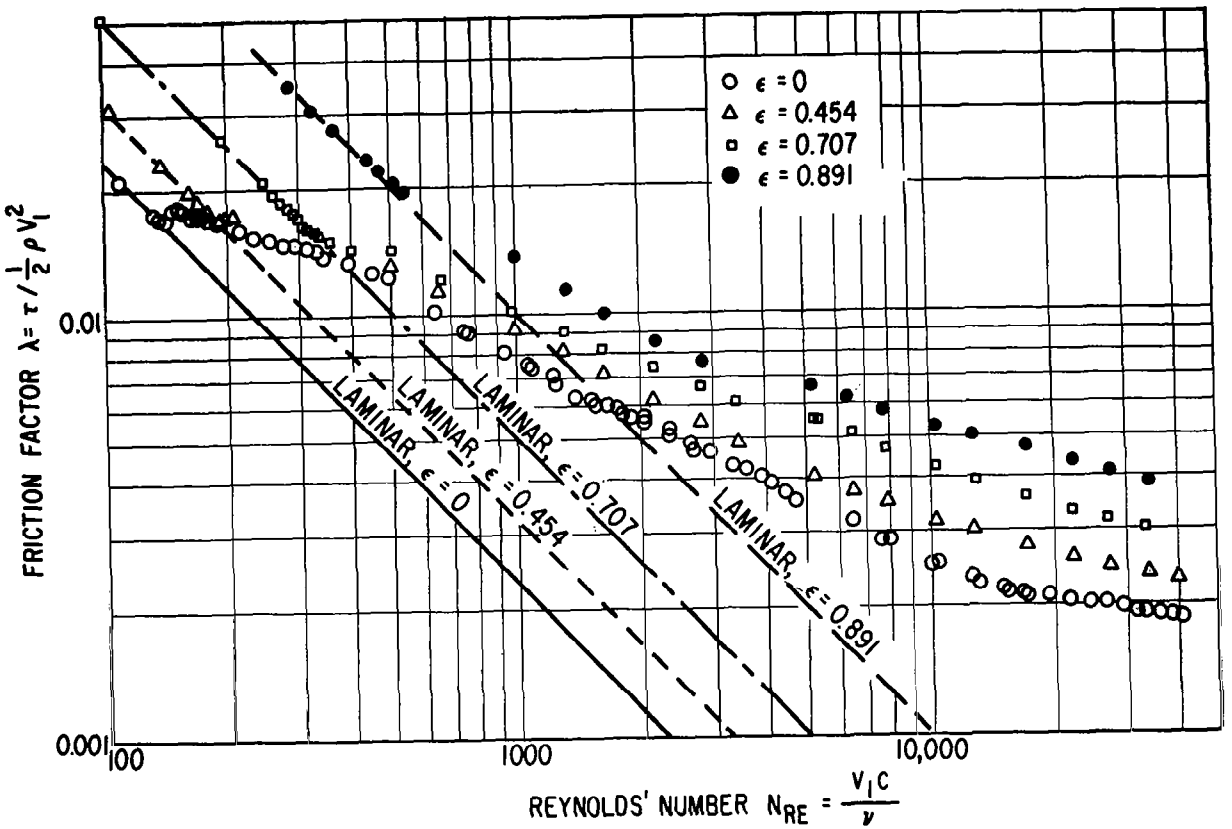

Figure 15. - Friction factor vs Reynolds number for flow between rotating cylinders at various eccentricity ratios; $C/R_1 = 0.099$.

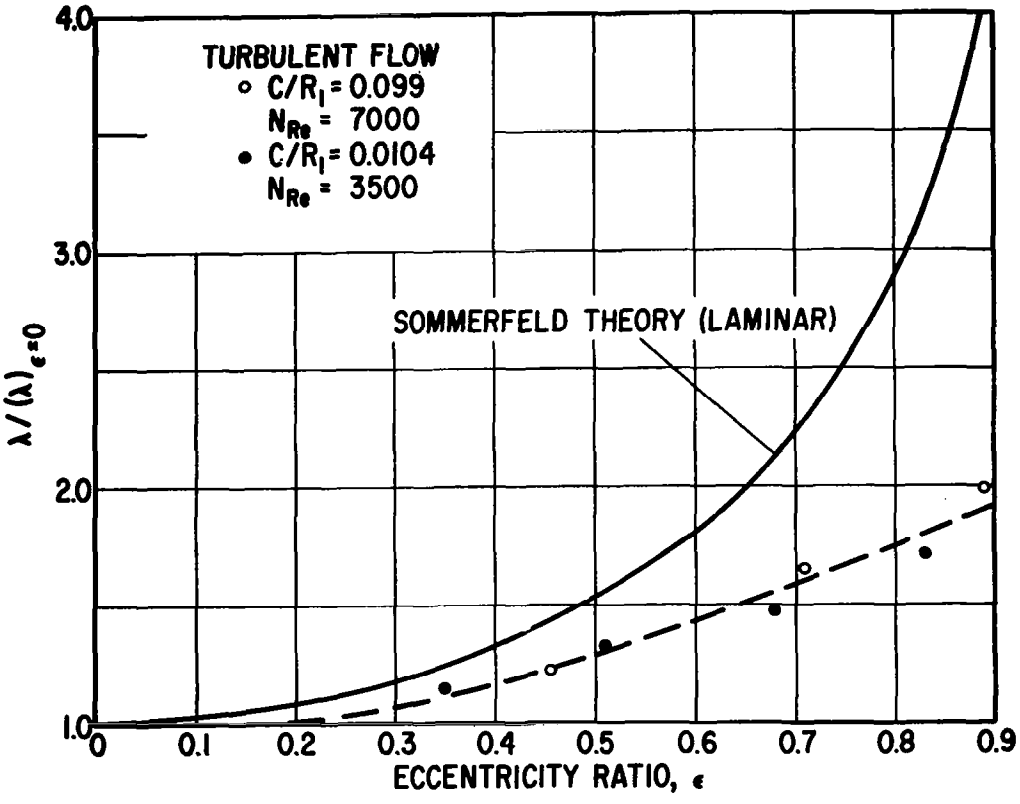

Figure 16. - Ratio of friction factor for non-concentric cylinders to friction factor for concentric cylinders.

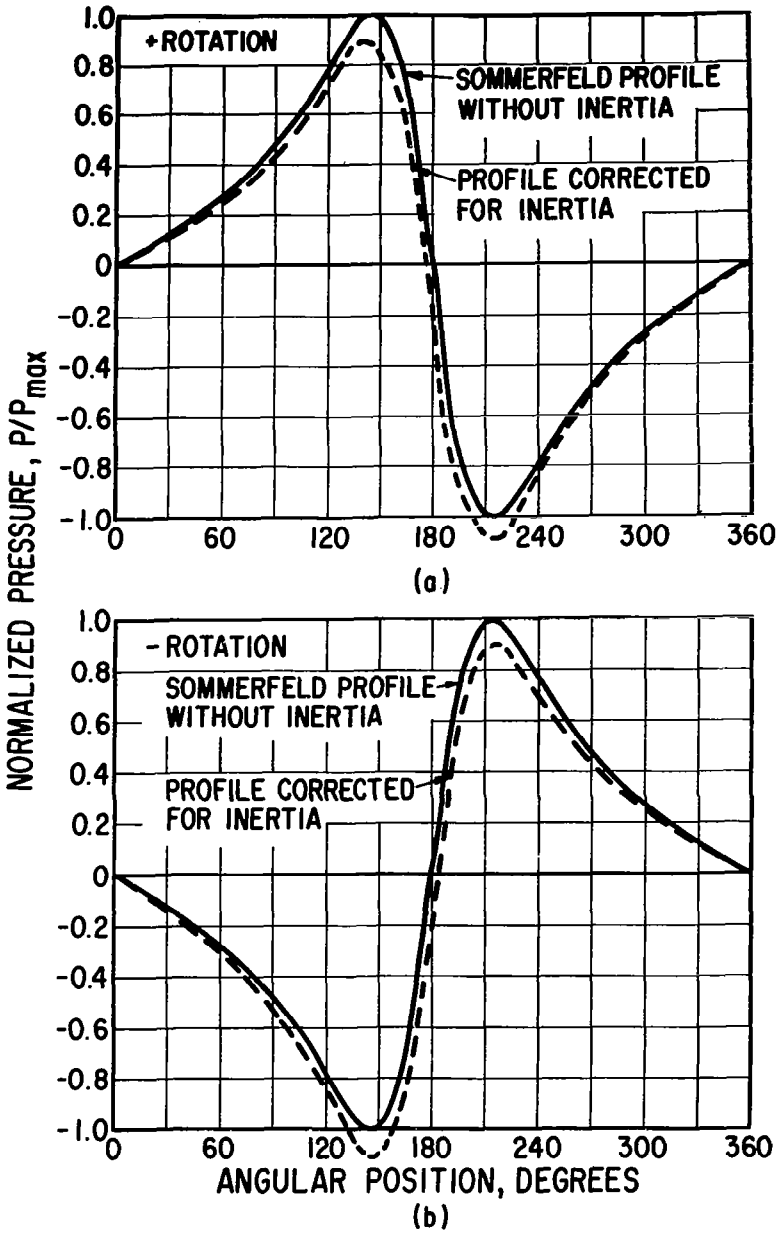

Figure 17. - Normalized schematic pressure profiles showing effect of fluid inertia.

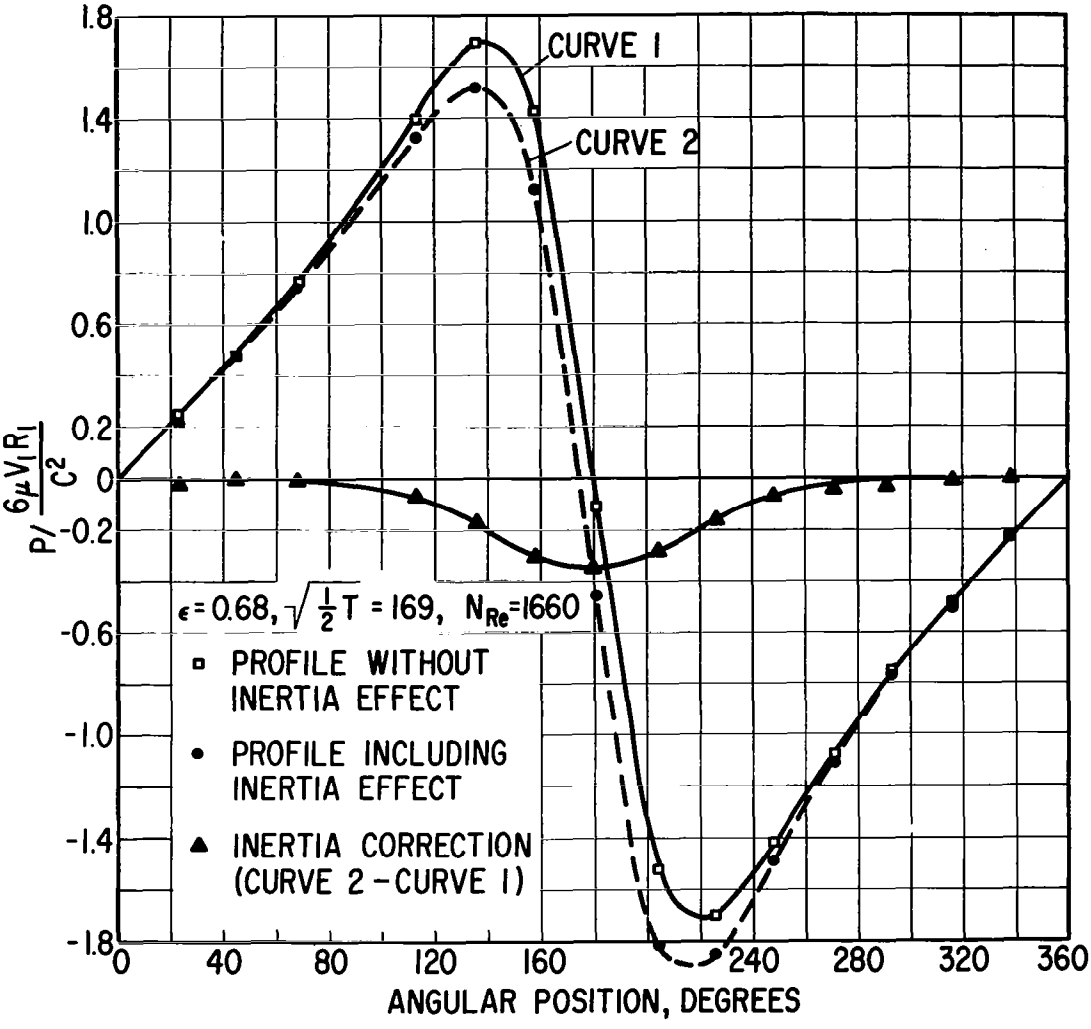

Figure 18. - Dimensionless pressure profiles with and without inertia effect for an eccentricity ratio of 0.68.

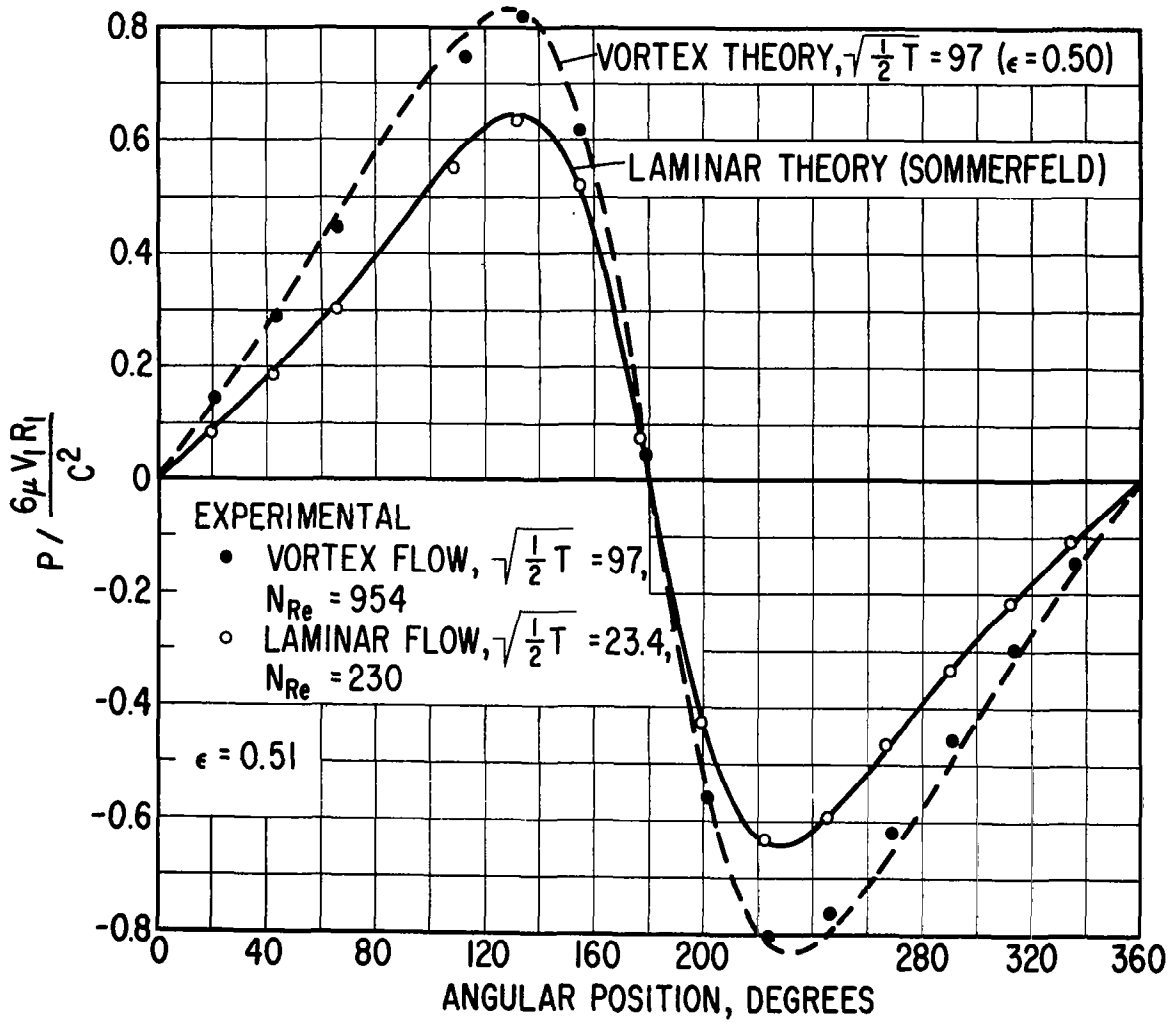

Figure 19. - Dimensionless pressure profiles for an eccentricity ratio of 0.51; comparison of experiment with theory.

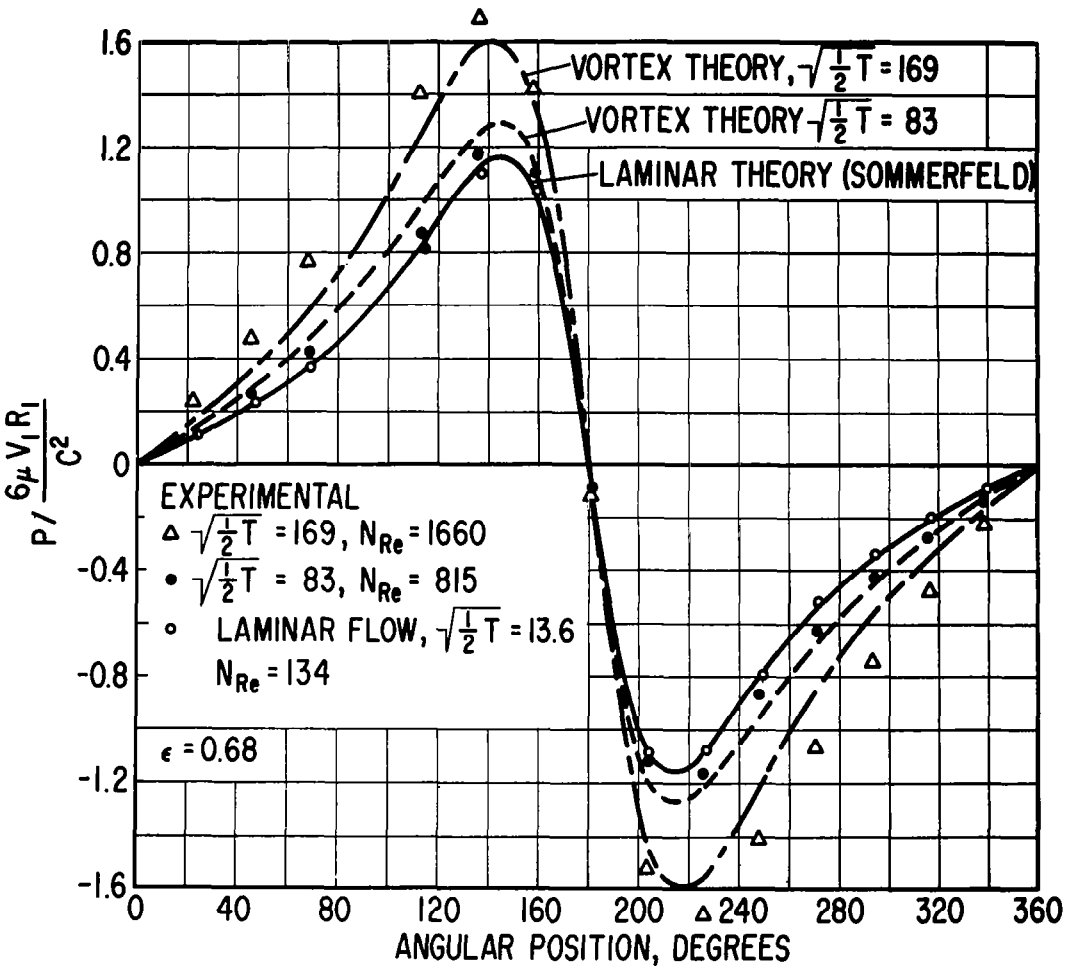

Figure 20. - Dimensionless pressure profiles for an eccentricity ratio of 0.68; comparison of experiment with theory.

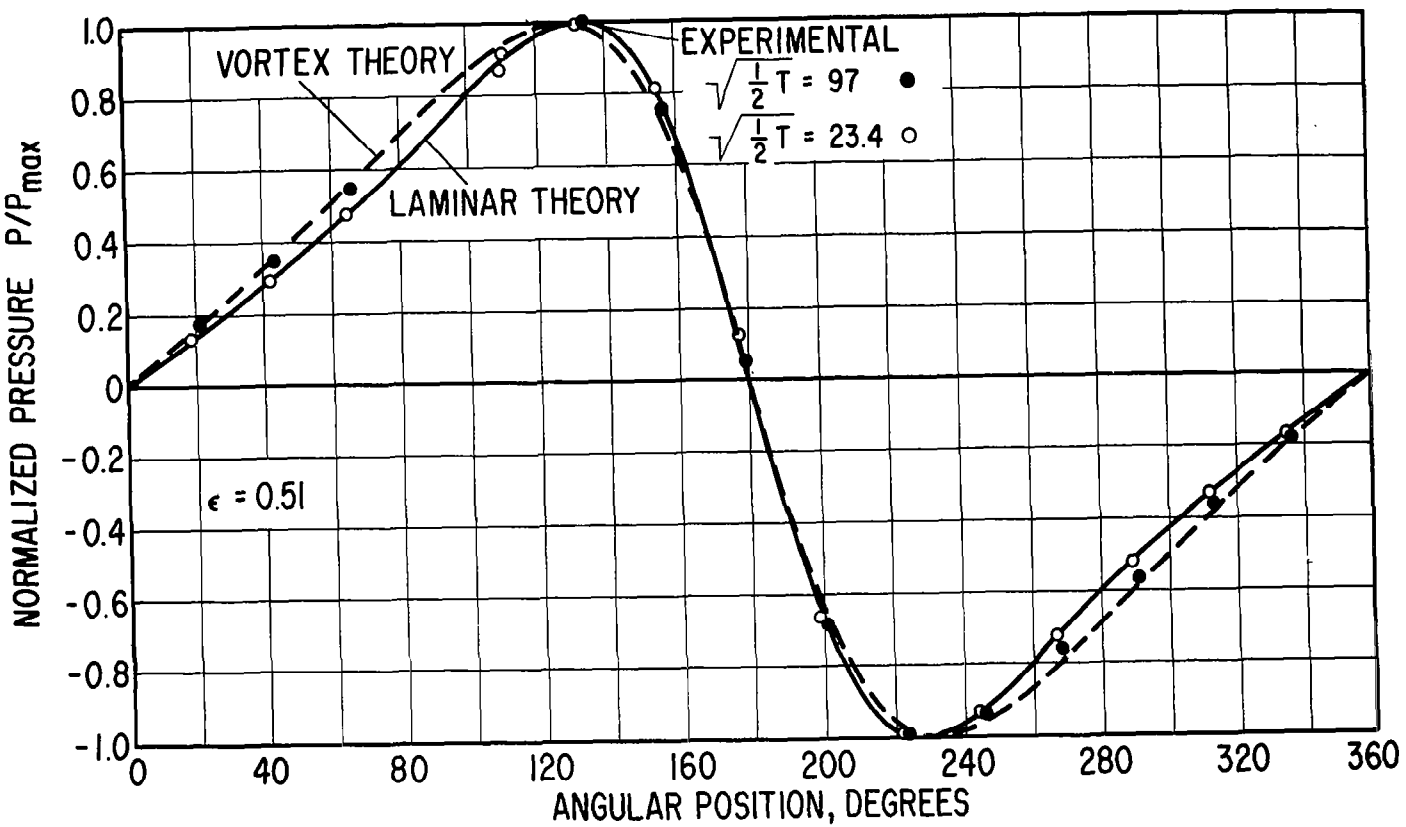

Figure 21. - Normalized pressure profiles; $\epsilon = 0.51$.

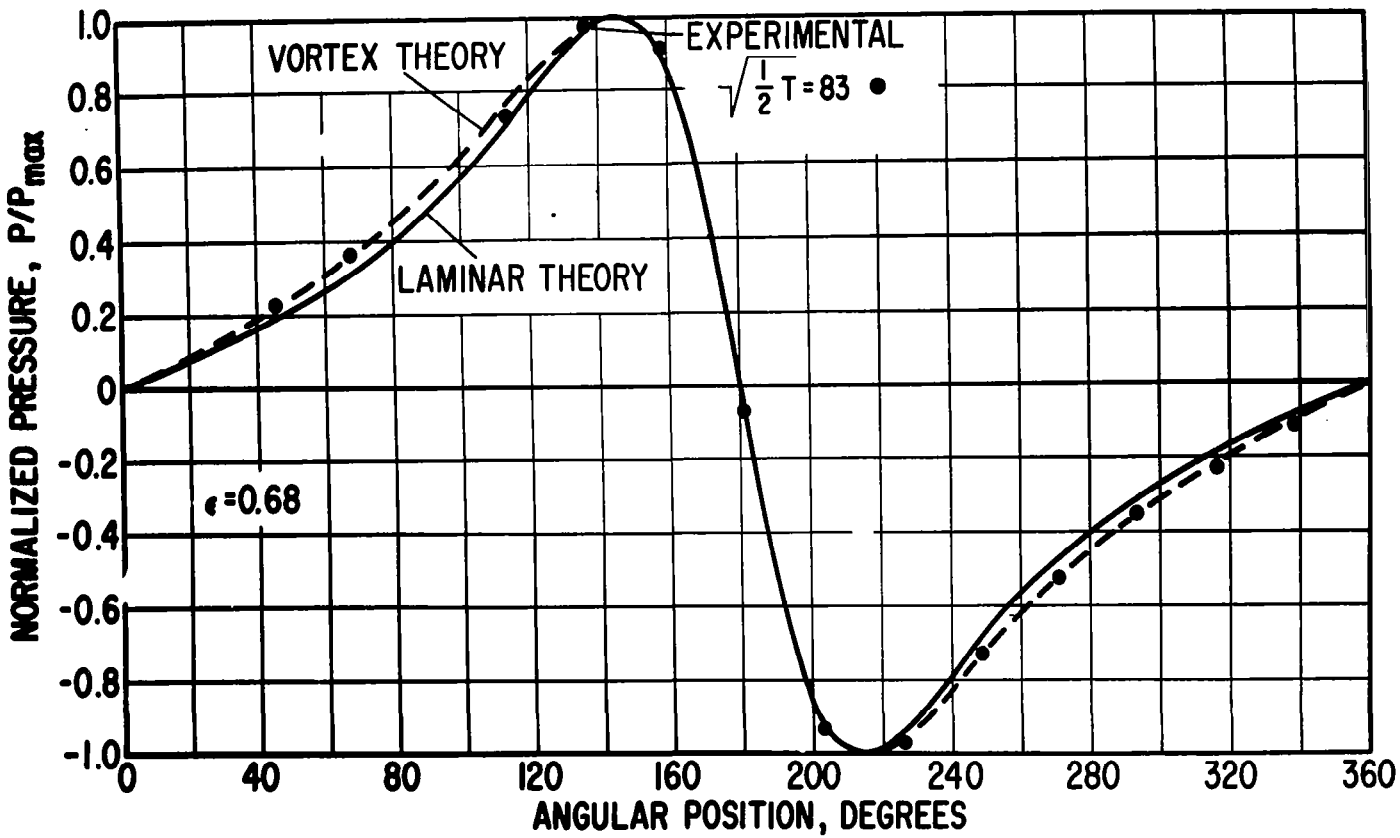

Figure 22. - Normalized pressure profiles; ϵ = 0.68.

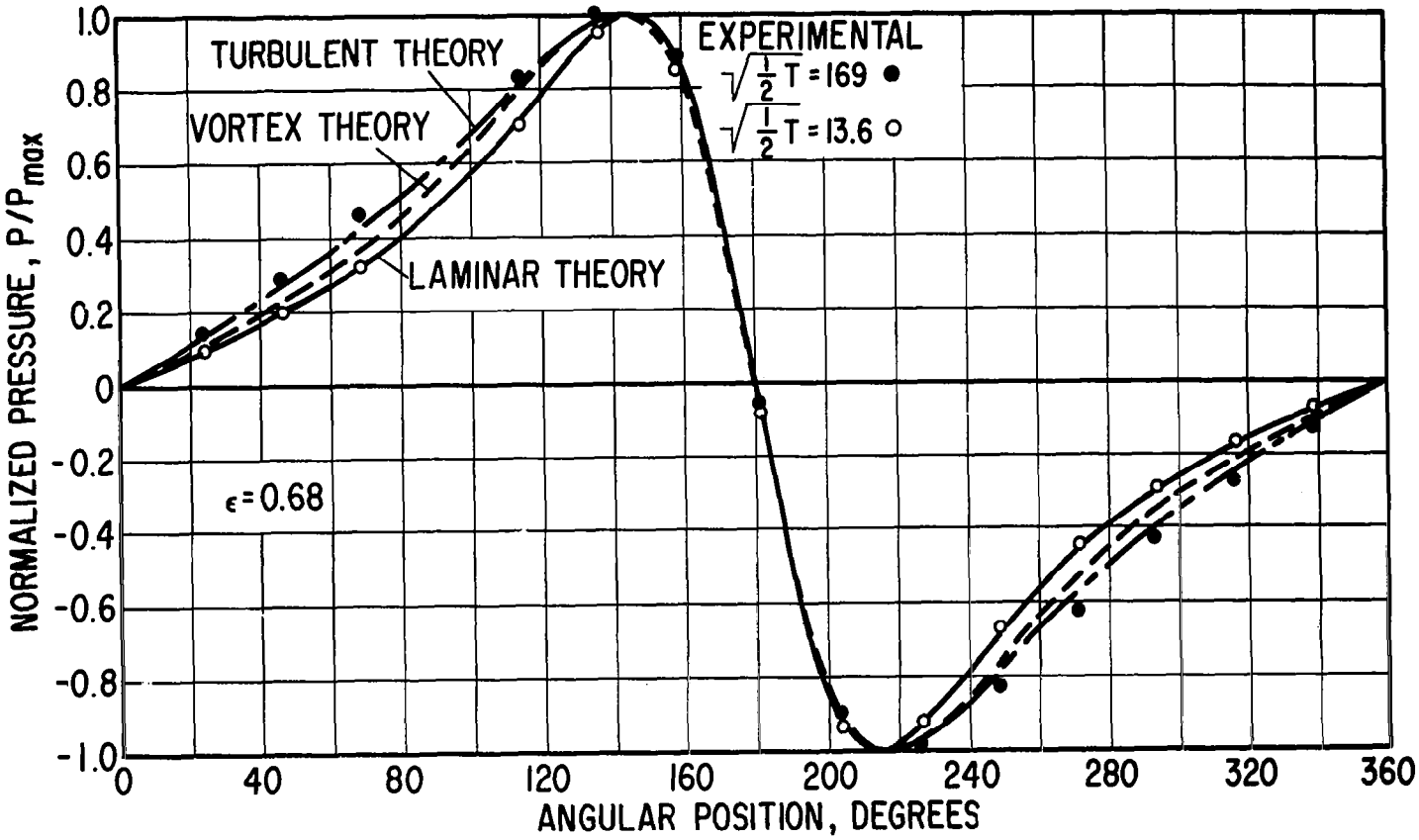

Figure 23. - Normalized pressure profiles; $\epsilon = 0.68$.

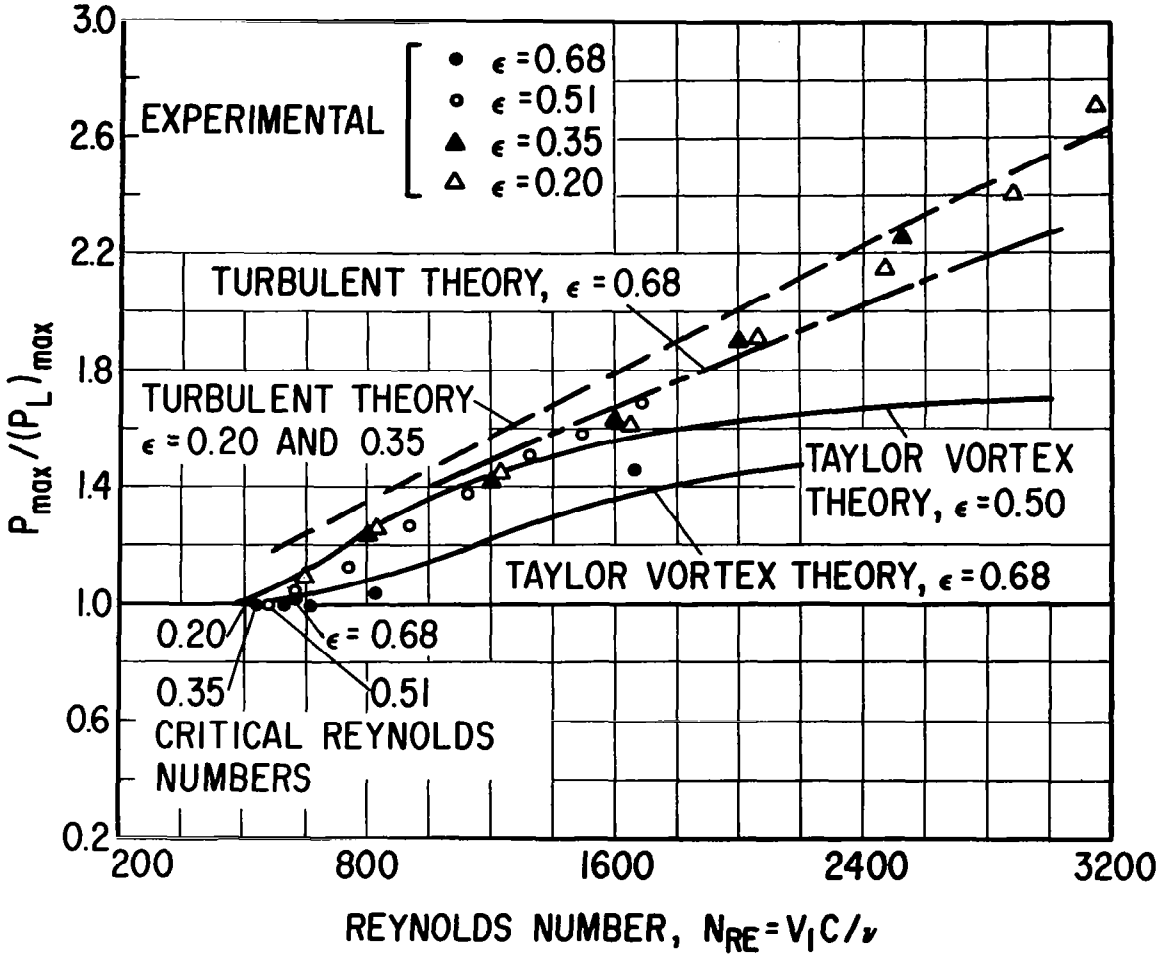

Figure 24. - Ratio of maximum pressure in superlaminar flow regime to maximum pressure that would occur if flow remained laminar. Critical Reynolds numbers shown indicate point of onset of vortices at different eccentricities.

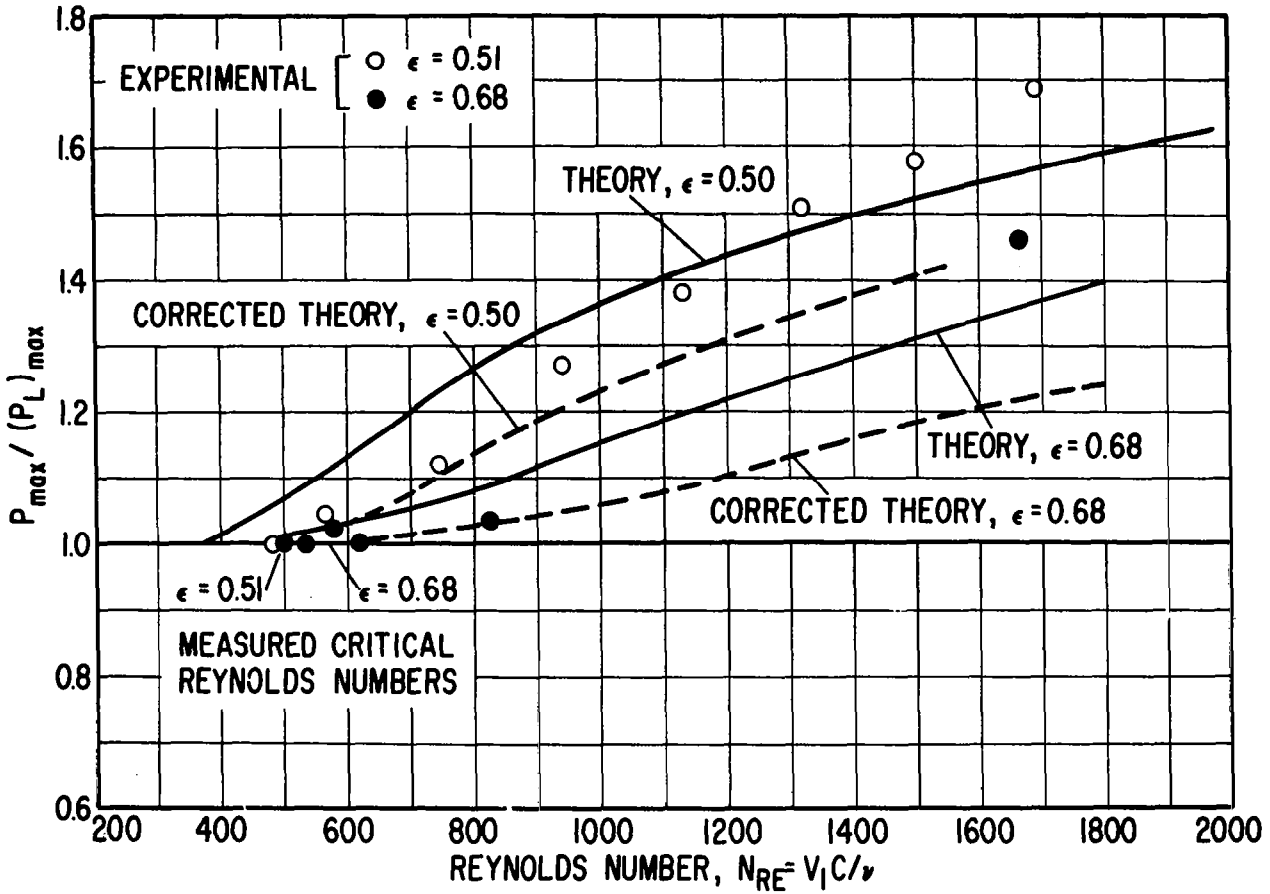

Figure 25. - Ratio of maximum pressure in superlaminar flow regime to maximum pressure that would occur if flow remained laminar. Measured critical Reynolds numbers shown indicate point of onset of vortices at $\epsilon = 0.51$ and $\epsilon = 0.68$.

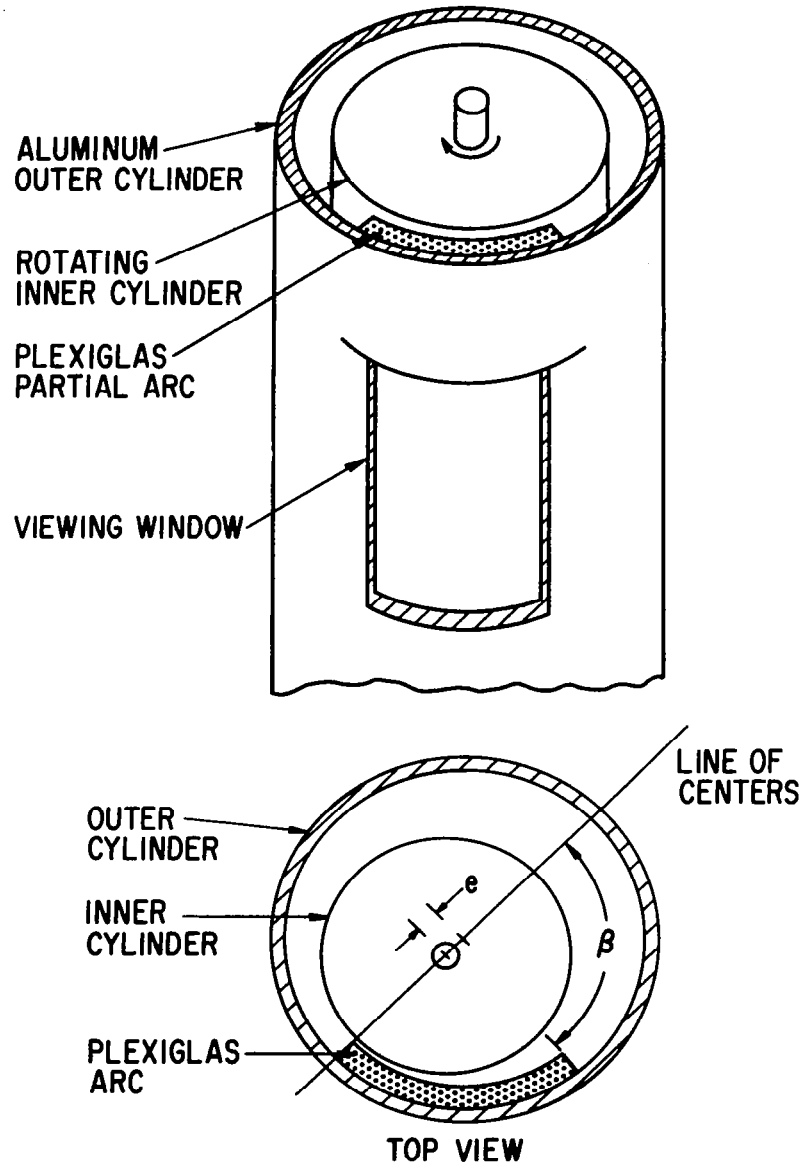

Figure 26. - Schematic drawing of partial-arc test cylinders.

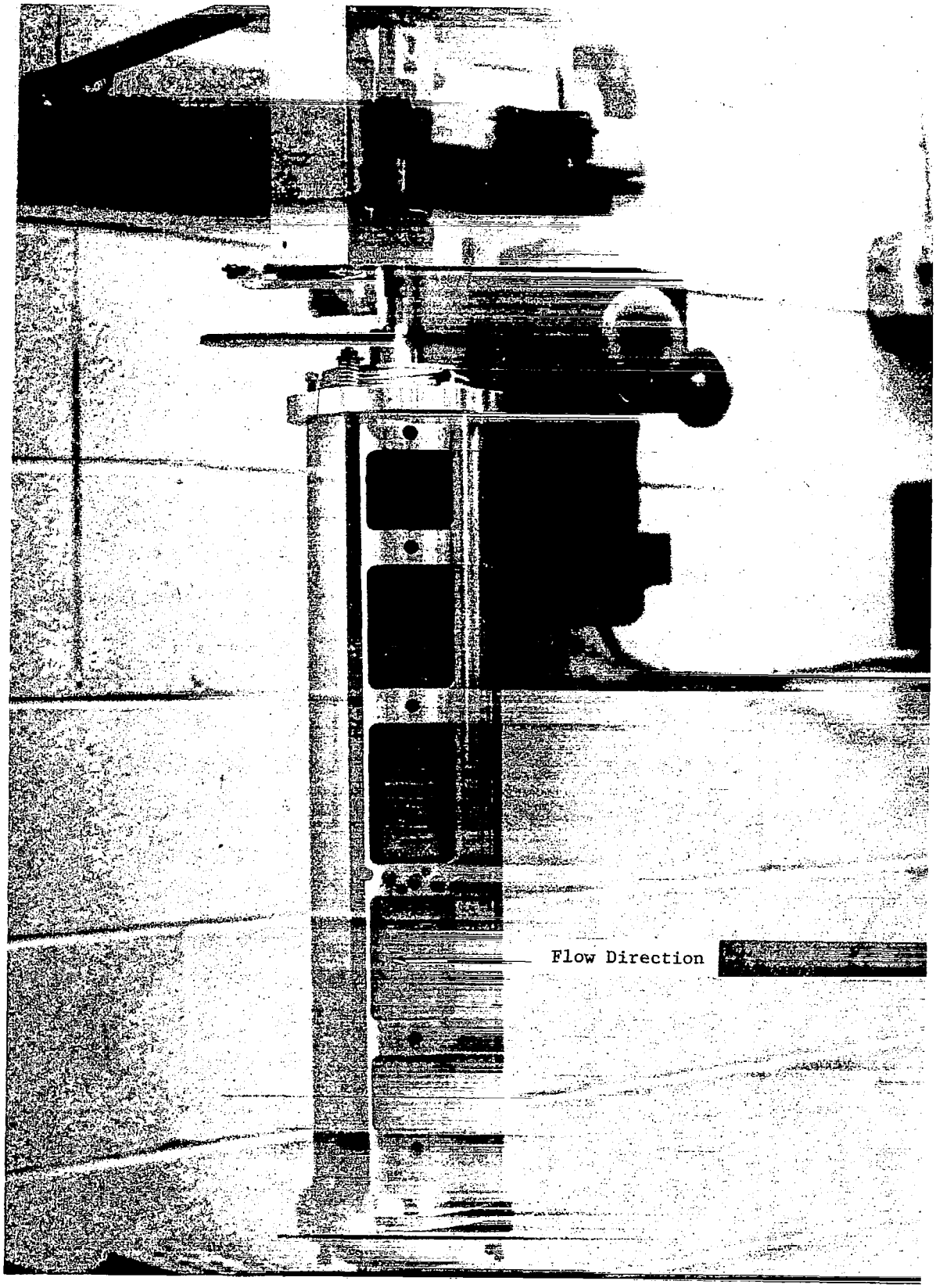

Figure 27. - Partial arc test rig.

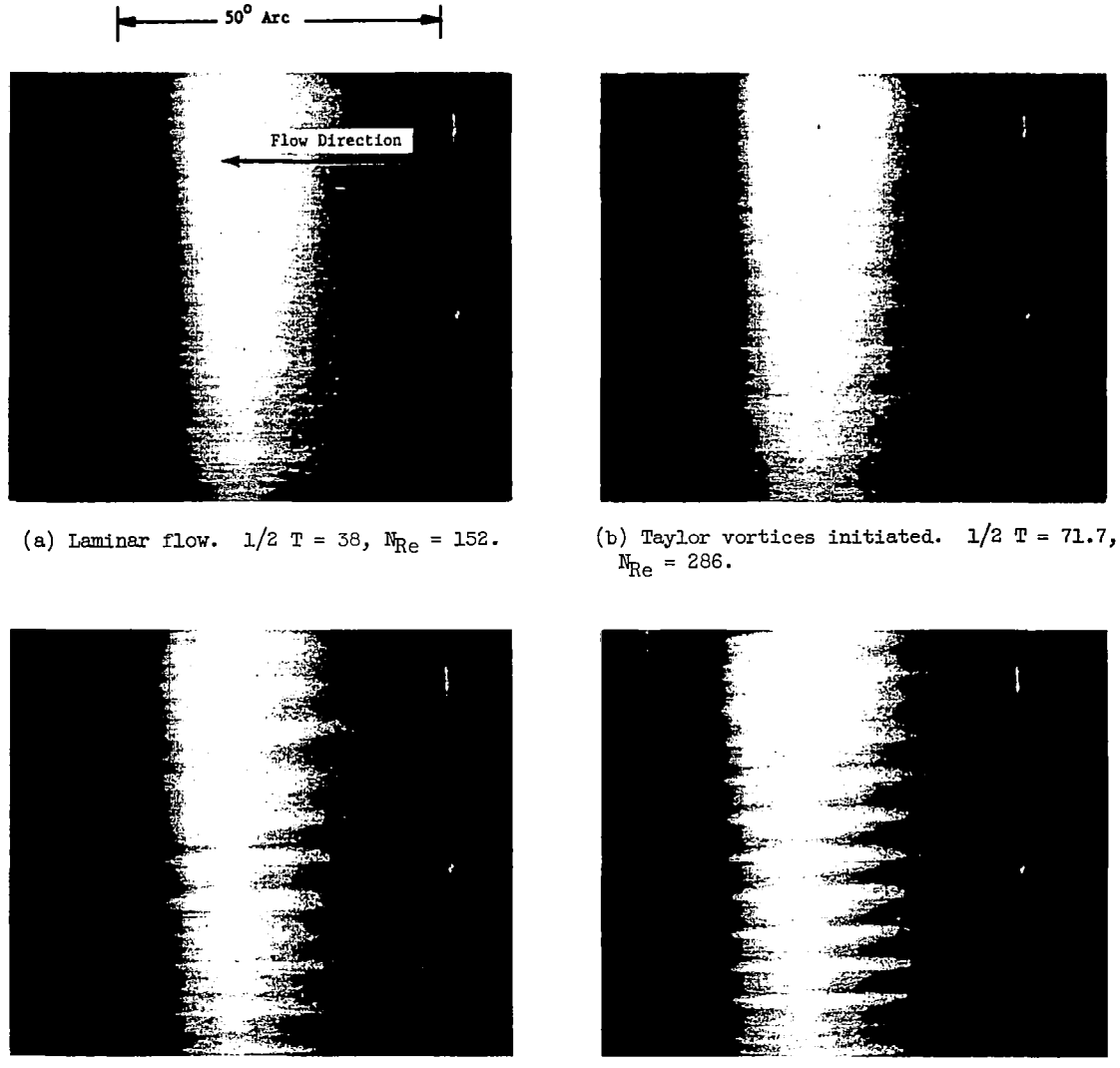

(a) Laminar flow. 1/2 T = 38, N_{Re} = 152.

(b) Taylor vortices initiated. 1/2 T = 71.7, N_{Re} = 286.

(c) Fully developed vortex flow. 1/2 T = 89, N_{Re} = 355.

(d) Fully developed vortex flow. 1/2 T = 105, N_{Re} = 419.

Figure 28. - Developing vortex flow in converging partial arc, ϵ = 0.706. Film thickness at start of arc (θ = 100°) = 0.136 in. Film thickness at end of arc (θ = 180°) = 0.049 in.

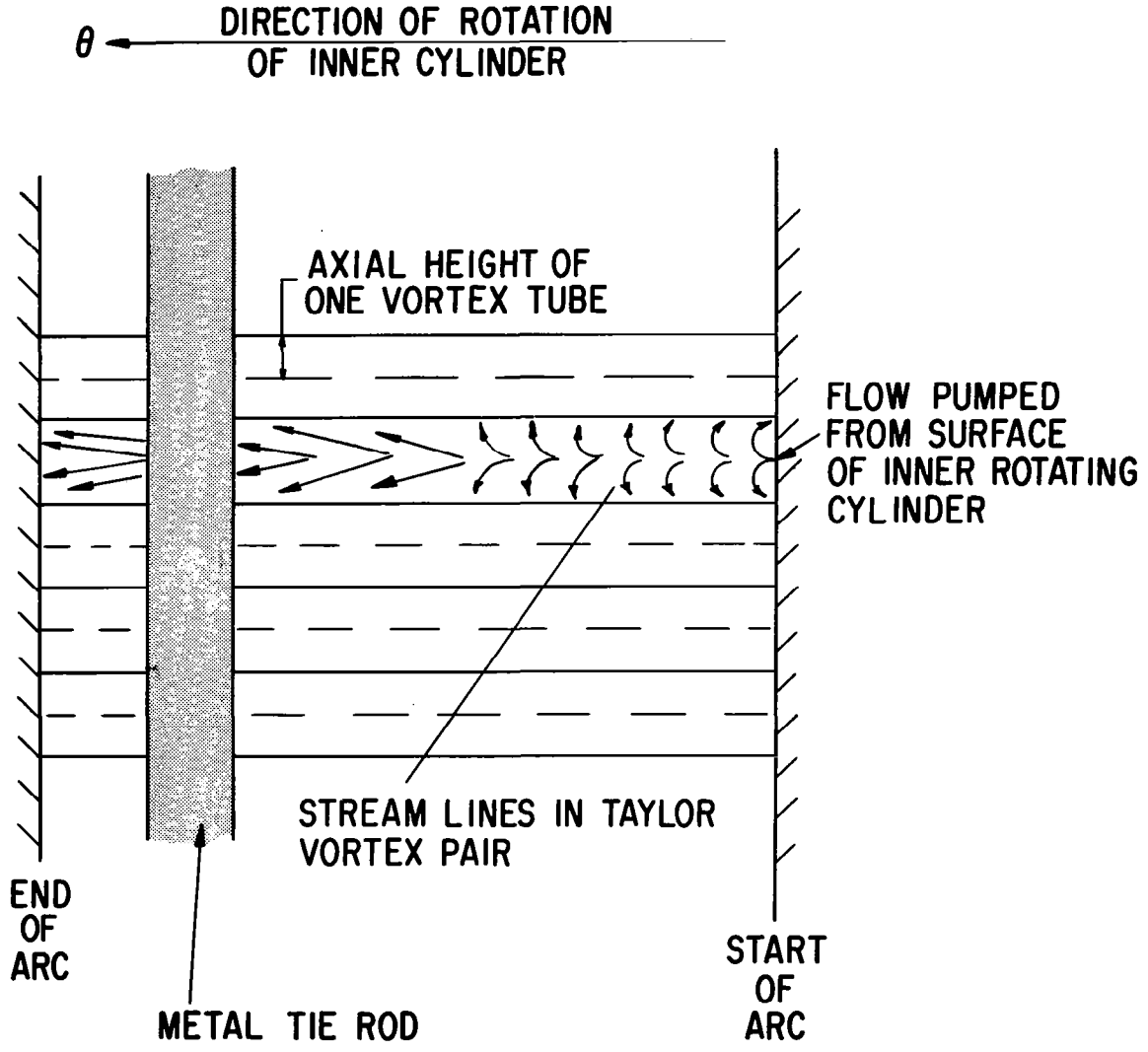

Figure 29. - Schematic diagram of vortex flow looking through transparent partial arc bearing.

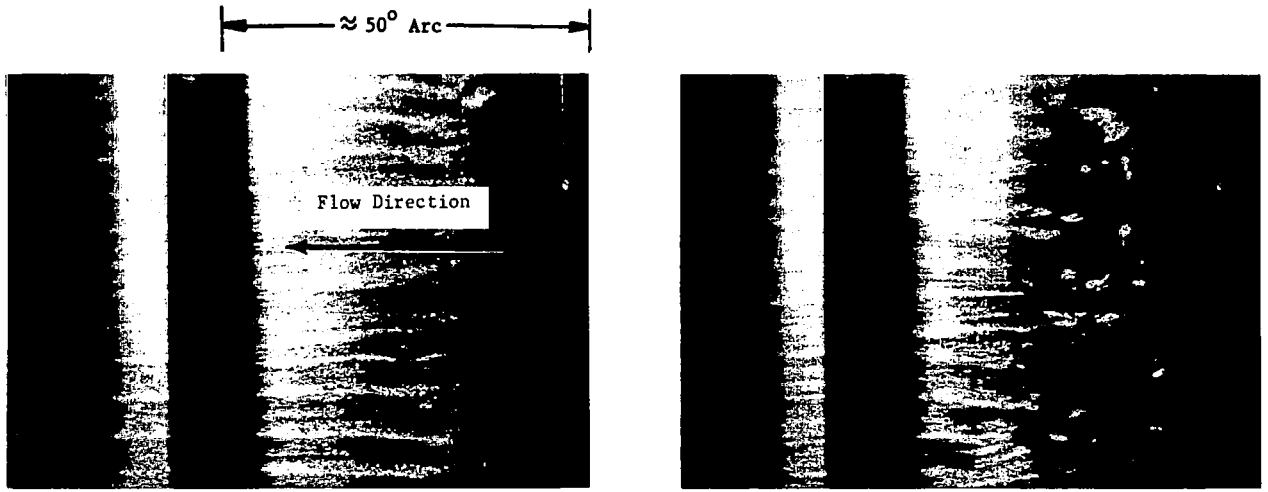

(a) Laminar vortex flow. N_{Re} = 524.

(b) Breakdown of regular vortex flow. N_{Re} = 1048.

(c) Turbulent flow at start of arc. N_{Re} = 1850.

(d) Turbulent flow throughout arc. N_{Re} = 4400.

Figure 30. - Developing turbulence in converging partial arc, ϵ = 0.706. Film thickness at start of arc (θ = 100°) = 0.136 in. Film thickness at end of arc (θ = 180°) = 0.049 in.

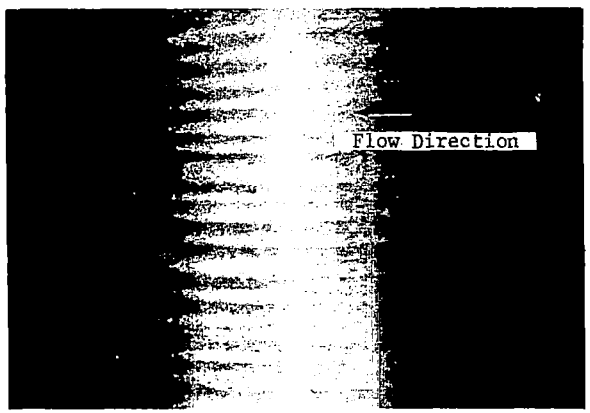

(a) Laminar vortex flow. N_{Re} = 705.

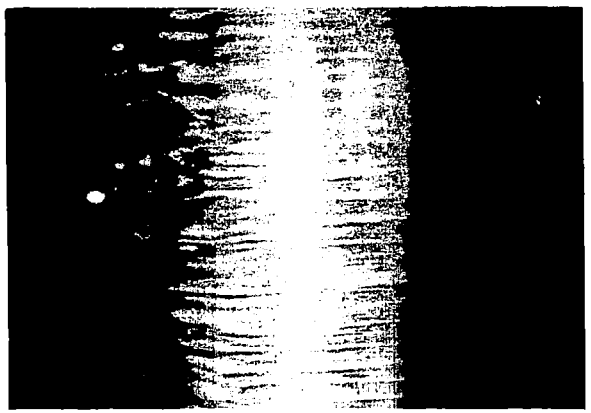

(b) Vortex flow with turbulence at end of arc. N_{Re} = 1160.

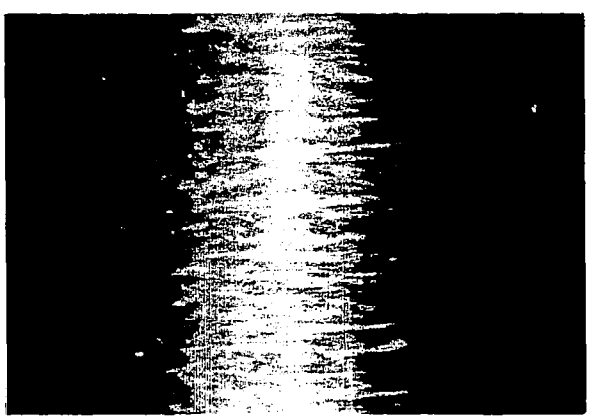

(c) Fully turbulent flow. N_{Re} = 2330.

Figure 31. - Developing turbulence in diverging partial arc, ϵ = 0.0706. Film thickness at start of arc (θ = 180°) = 0.049 in. Film thickness at end of arc (θ = 260°) = 0.136 in.

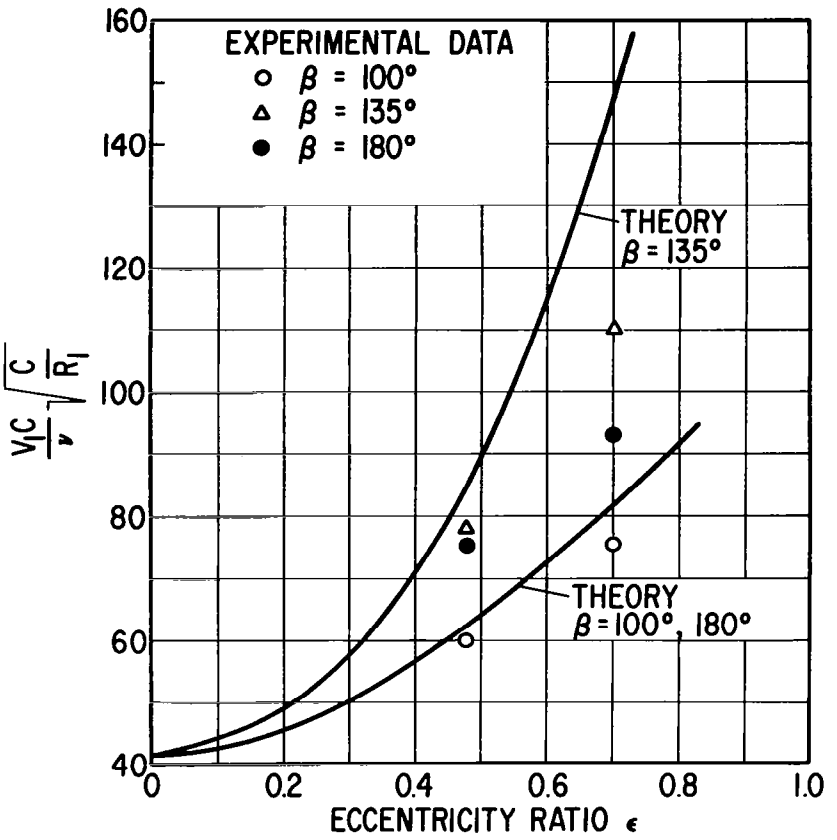

Figure 32. - Transition speeds for onset of vortices in flow between rotating inner cylinder and partial-arc outer cylinder.

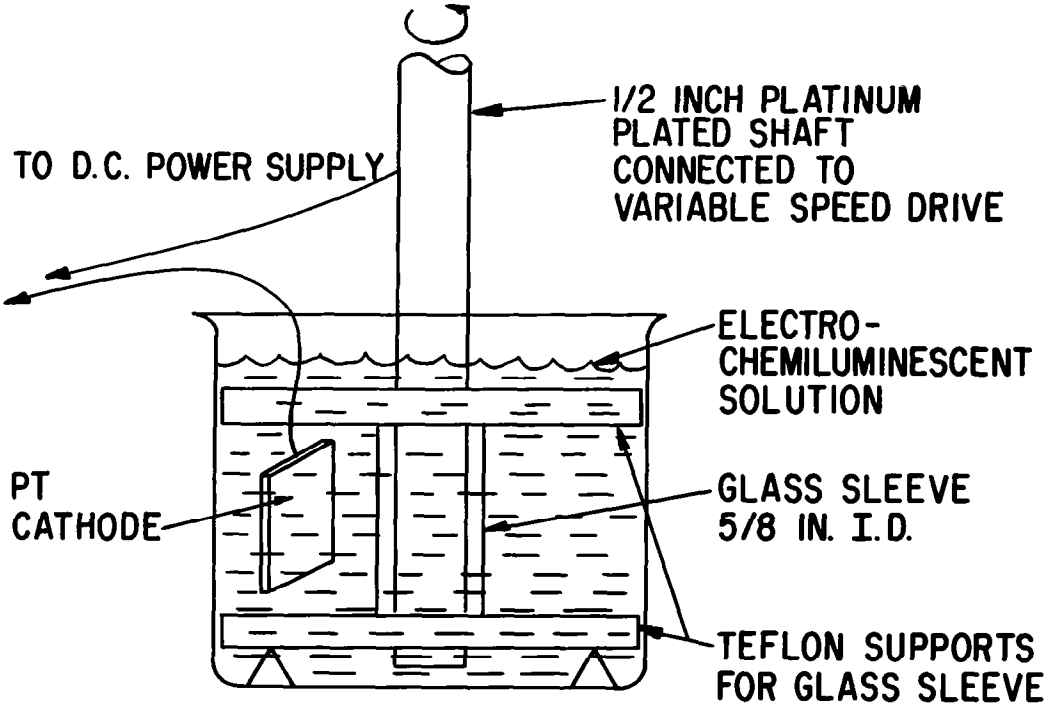

Figure 33. - Schematic of apparatus for electrochemiluminescence studies.

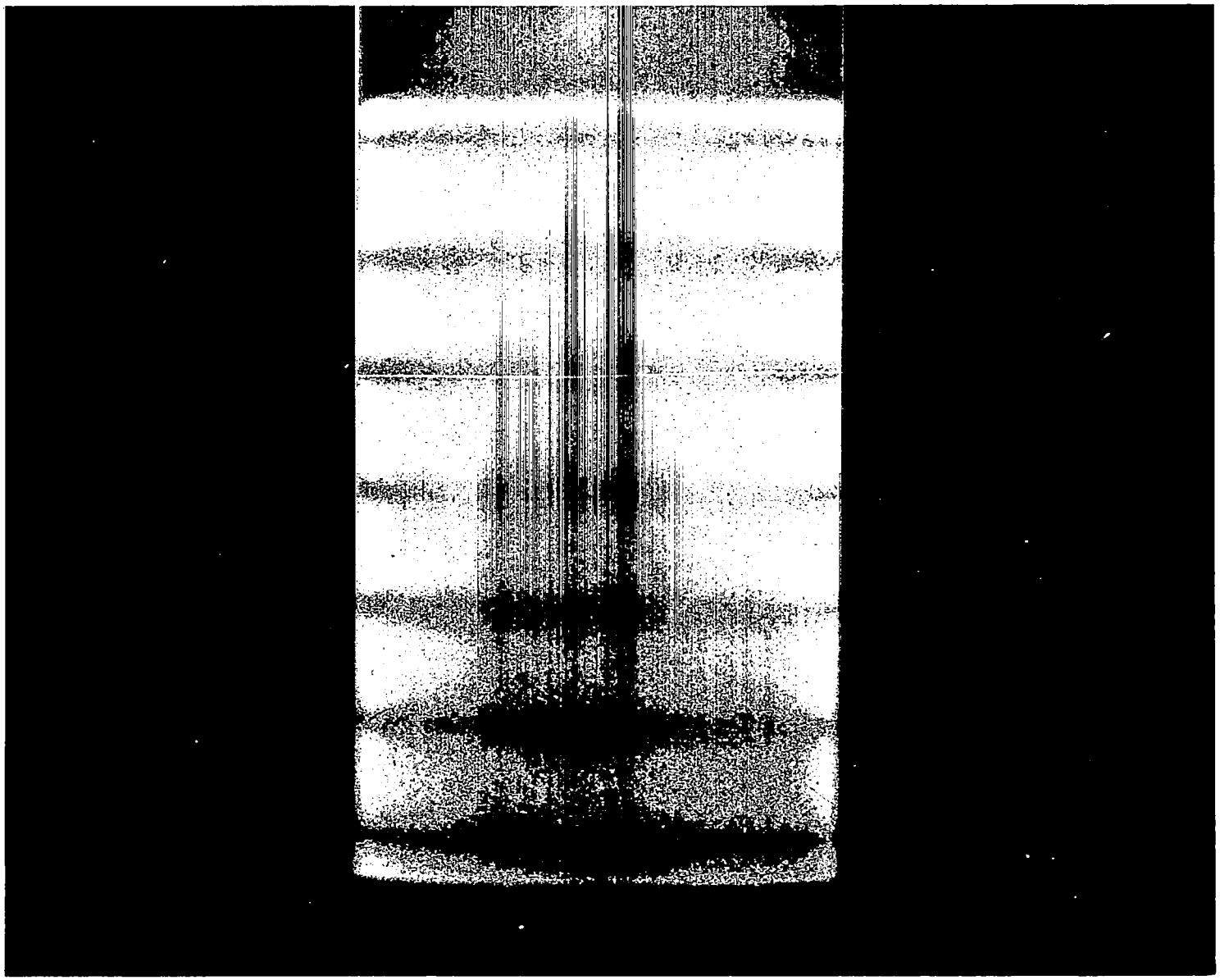

Figure 34. - Photograph of Taylor vortex flow pattern made visible by electrochemiluminescence.